MAGNETIC RESONANCE IMAGING OF CEREBRAL VENOUS OXYGENATION

APPROVED BY SUPERVISORY COMMITTEE

Hanzhang Lu, Ph.D.

Ralph P. Mason, Ph.D.

Ananth Madhuranthakam, Ph.D.

Masaya Takahashi, Ph.D.

DEDICATION

To my mentor, Professor Hanzhang Lu, Ph.D., who has taught me all the things I need to survive in the jungle.

To my family for their loyal love and support.

MAGNETIC RESONANCE IMAGING OF CEREBRAL VENOUS OXYGENATION

by

DENG MAO

DISSERTATION

Presented to the Faculty of the Graduate School of Biomedical Sciences

The University of Texas Southwestern Medical Center at Dallas

In Partial Fulfillment of the Requirements

For the Degree of

DOCTOR OF PHILOSOPHY

The University of Texas Southwestern Medical Center at Dallas

Dallas, Texas

May, 2017

MAGNETIC RESONANCE IMAGING OF CEREBRAL VENOUS OXYGENATION

Publication No. _____

Deng Mao, Ph.D.

The University of Texas Southwestern Medical Center at Dallas, 2017

Hanzhang Lu, Ph.D.

Cerebral venous oxygenation (Y_v) is an important biomarker for brain diseases. My dissertation consisted of two studies. The first study aims to investigate the regional Y_v in hypertension. Hypertension is known to cause cerebral hypoperfusion and cortical atrophy but its impact on Y_v is not yet clear. A 2D venous oxygenation mapping technique, TRUPC was applied to an elderly cohort from Dallas Heart Study. The Y_v in internal cerebral veins (ICV), anterior and posterior superior sagittal sinus (SSS) and anatomical data was obtained. It was found lower relative venous oxygenation in the ICV and anterior SSS are associated with high systolic pressure. Such trend is also observed in hypertensive group alone. Moreover, the volume reduction in hippocampus and thalamus is correlated with decreased regional Y_v. The findings presented are consistent with previous literature on the targeted hypofusion and volume reduction in these regions. Imaging marker Y_v reported here may

prove valuable in the understanding of hypoxia effect, hypoperfusion and cortical volume reduction caused by hypertension.

The second study aims to develop an R_2^*-based MR oximetry that can measure cerebral Y_v in 3D. This technique separates blood signal from tissue by velocity-encoding phase contrast and measures the R_2^* of pure blood by multi-gradient-echo acquisition. The blood R_2^* was converted to Y_v using an R_2^*-vs-oxygenation (Y) calibration curve, which was obtained by in vitro bovine blood experiments. Reproducibility, sensitivity, validity, and resolution dependence of the technique were evaluated. In vitro R_2^*-Y calibration plot revealed a strong dependence of blood R_2^* on oxygenation, with additional dependence on hematocrit. In vivo results demonstrated that the technique can provide a 3D venous oxygenation map that depicts both large sinuses and smaller cortical veins, with venous oxygenation ranging from 57% to 72%. Intra-session coefficient-of-variation of the measurement was 3.0%. The technique detected an average Y_v increase of 10.8% due to hyperoxia, which was validated by global oxygenation measurement from TRUST. Two spatial resolutions, one with an isotropic voxel dimension and the other with a non-isotropic dimension, were tested for full brain coverage. This study demonstrated the feasibility of 3D brain oxygenation mapping without using contrast agent.

TABLE OF CONTENTS

PRIOR PUBLICATIONS

Mao D, Li Y, Liu P, Peng S, Lu H. Three-dimensional mapping of brain venous oxygenation using R2* oximetry. Under second round review at Magn Reson Med..

Sheng M, Liu P, Mao D and Lu H, Hyperoxia suppresses resting-state electroencephalography (EEG) activity and causes temporal delays in task-evoked potentials. In press at PLoS One.

Su P, Mao D, Liu P, Li Y, Pinho M, Welch BG and Lu H. Multi-parametric estimation of brain hemodynamics with MR Fingerprinting ASL (MRF-ASL). In press at Magn Reson Med..

Gopal K, Thomas BP, Nandy R, Mao D and Lu H. Potential Audiological and MRI Markers of Tinnitus. In press at J Am Acad Audiol..

Krishnamurthy LC, Mao D, King KS, Lu H. Correction and optimization of a T2-based approach to map blood oxygenation in small cerebral veins. Magn Reson Med. 2016;75(3):1100-9.

Wang GZ, Belgard TG, Mao D, Chen L, Berto S, Preuss TM, Lu H, Geschwind DH, Konopka G. Correspondence between Resting-State Activity and Brain Gene Expression. Neuron. 2015;18;88(4):659-66.

Gopal KV, Thomas BP, Mao D, Lu H. Efficacy of carnitine in treatment of tinnitus: evidence from audiological and MRI measures-a case study. J Am Acad Audiol. 2015;26(3):311-24.

Pascual JM, Liu P, Mao D, Kelly DI, Hernandez A, Sheng M, Good LB, Ma Q, Valencia I, Zhang X, Park JY, Hynan LS, Stavinoha P, Roe CR, Lu H. Triheptanoin for glucose transporter type I deficiency (G1D): modulation of human ictogenesis, cerebral metabolic rate, and cognitive indices by a food supplement. JAMA Neurol. 2014; 71(10):1255-65.

Tung KC, Uh J, Mao D, Xu F, Xiao G, Lu H. Alterations in resting functional connectivity due to recent motor task. Neuroimage. 2013; 78:316-24.

LIST OF FIGURES

LIST OF TABLES

LIST OF DEFINITIONS

ASL: Arterial Spin Labeling

BOLD: Blood Oxygenation Level Dependent

CBF: Cerebral Blood Flow

CBV: Cerebral Blood Volume

$CMRO_2$: Cerebral Metabolism Rate of Oxygen

EEG: Electroencephalogram

ICV: Internal Cerebral Veins

MPRAGE: Magnetization-Prepared Rapid Gradient-Echo

MRI: Magnetic Resonance Imaging

OEF: Oxygenation Extraction Fraction

PET: Positron Emission Tomography

QUIXOTIC: QUantitative Imaging of eXtraction of Oxygen and Tissue Consumption

ROI: Region Of Interest

SSS: Superior Sagittal Sinus

TRUPC: T_2-Relaxation-Under-Phase-Contrast

TRUST: T_2-Relaxation-Under-Spin-Tagging

VSEAN: Velocity-Selective Excitation with Arterial Nulling

Y: Oxygenation, fraction of saturated hemoglobin to total hemoglobin

Y_a: Arterial oxygenation

Y_v: Venous oxygenation

CHAPTER ONE

Introduction

Cerebral venous oxygenation is defined as the fraction of the oxygenated hemoglobin to the total hemoglobin in the venous blood of the brain. The first question to ask is, "why do we need to measure cerebral venous oxygenation?" It all starts with the oxygen metabolism of the brain. Our brains equip us with marvelous cognitive function, but good things often come with a high cost. Our brains rely heavily on the oxygenation metabolism to provide sufficient energy for their normal function. The brain constitutes 2% of the total body weight, but consumes 20% of the total energy (Attwell & Laughlin, 2001), mostly in aerobic way. Thus, the metabolism of brain is highly oxygen dependent. The oxygen supply to the brain can be either the cause or the effect of the conditions of the brain. The disturbance of oxygenation supply, like stroke, can affect brain's health, and in reverse way, the diseases in the brain can alter the oxygen metabolism of brain, like dementia (Thomas et al., 2016). Venous oxygenation is directly related to an indicator of the oxygen metabolism, oxygen extraction fraction (OEF). OEF is the difference between arterial oxygenation and venous

oxygenation divided by arterial oxygenation. OEF has been found to be associated with the health of the brain in various clinical studies, including stroke (Derdeyn et al., 2001; Gupta et al., 2014), tumor (Leenders, 1994) and Alzheimer's disease (Ishii et al., 1996; Nagata et al., 2000; Thomas et al., 2016). OEF has also been linked to brain function. For example, the concept of default mode network was first formed with OEF (Raichle et al., 2001). In addition to its relationship with OEF, cerebral venous oxygenation is one critical component of the delicate blood oxygenation level dependence (BOLD) model (Hoge et al., 1999). Functional MRI reveals the brain function and neural activity by measuring the change of BOLD signal. In a nut shell, measurement of cerebral venous oxygenation provides a window to study physiology, pathology, and function of our mysterious brain. This is the initiative of my following study aims.

My dissertation is divided into six parts, including this introduction chapter. In the following chapters, Chapter two will provide a brief overview of the current venous oxygenation measurement methods. Chapter three will be focusing on a clinical application of a 2D venous oxygenation measurement method using magnetic resonance imaging (MRI), TRUPC (Krishnamurthy et al., 2014a), to study the regional venous oxygenation in hypertension. Chapter

four will describe a novel three-dimensional mapping method of cerebral venous oxygenation using R_2^* oximetry developed by me. Chapter five will be on my other efforts to look at the neural activity using resting state functional MRI and electroencephalogram (EEG). In Chapter six, I will summarize the previous chapters and offer my final thoughts on further directions.

CHAPTER TWO

Current venous oxygenation measurement methods

Methods before MRI

Measuring the cerebral venous oxygenation has been of long interest of clinicians and scientists. Before the emergence of MRI techniques, there were two major ways to measure the cerebral venous oxygenation. The first one is catheter based method. The catheter based method is the most direct method. In this method, a catheter is installed in the internal jugular vein. The internal jugular veins virtually drain all the venous blood from the brain. The venous oxygenation can be yielded by using a blood gas analyzer to measure the blood drawn from the catheter (Macmillan & Andrews, 2000). A catheter based reflectance pulse oximetry can also be inserted in the internal jugular vein for continuous monitoring of the venous oxygenation (Schell & Cole, 2000). However, each of the internal jugular veins receives the blood from both hemispheres, so this method is still a purely global measurement. Inserting the catheter can be invasive, which can explain why it is not used in the routine

clinical procedure. Its usage is limited in the critical care settings (Schell & Cole, 2000).

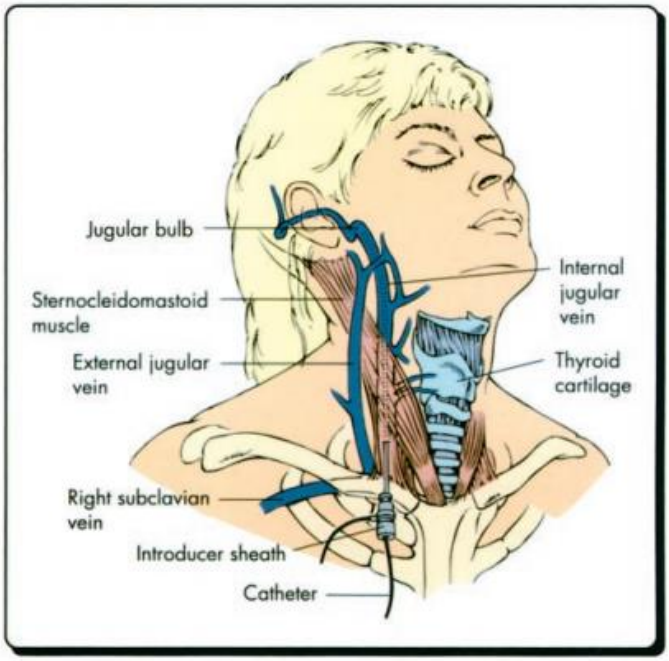

Figure 2-1: The placement of catheter to sample the blood in the internal jugular vein. The figure is adapted from (Schell & Cole, 2000).

Another cerebral oxygenation measurement method is the ^{15}O positron emission tomography (PET) method (Mintun et al., 1984). The PET method is still the reference standard for venous oxygenation measurement. PET is a functional imaging method based on the introduction of radioactive isotopes to the body. The PET system detects the gamma ray from the annihilation of positron emitted by the isotopes, in this case, ^{15}O. The method is based on a

two-compartment model, as shown in Figure 2-2. The model assumes the $^{15}O_2$ in the intravascular compartment on the left will exchange with the tissue compartment on the right. Once entered the tissue compartment, the labeled oxygen is immediately metabolized in to $H_2{}^{15}O$. The fraction of the $^{15}O_2$ entered tissue is related to venous oxygenation in a given region. But simple model doesn't mean it is easy to perform such method. The method consists of three scans: Injection of ^{15}O labeled water to measure cerebral blood flow (CBF), inhalation of $C^{15}O$ to determine cerebral blood volume (CBV) and a third scan of inhalation of $^{15}O_2$. It also requires the sampling of arterial blood for the tracer concentration. On the other hand, the ^{15}O has a short half-life of 112 s and requires an onsite cyclotron for preparation. Thus, the complexity and the high cost of this method has limited its application.

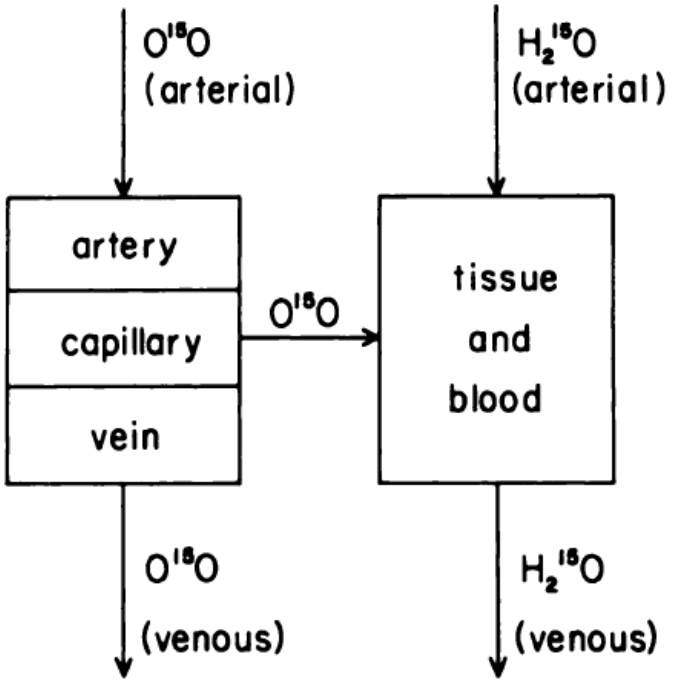

Figure 2-2: The two-compartment model of ^{15}O PET. The figure is adapted from (Mintun et al., 1984).

The near infrared spectroscopy (NIRS) is also a popular and non-invasive method to monitor tissue oxygenation clinically. Deoxygenated and oxygenated hemoglobins have difference light absorption abilities, which cause the different color between the bright red arterial blood and dark red venous blood visually. While the visible light has limited penetration through the skull, the near infrared light with a longer wavelength can penetrate through skull and reach the cortex at a depth up to ~1.7 cm (Murkin & Arango, 2009). In theory

(Murkin & Arango, 2009), the concentration of the substance X, [X] can be calculated from Beer-Lambert law: $[X]=\Delta A/L\times\varepsilon$. ΔA is the amount of light absorption, L is the photon path-length through the tissue and ε is the extinction coefficient for the wavelength of the light used and is substance specific. ε can be measured for both oxyhemoglobin and deoxyhemoglobin at different wavelengths, as shown in Figure 2-3. ΔA is measured by NIRS. L is unknown. So absorption at multiple wavelengths needs to be measured in order to calculate oxygenation. In commercial NIRS, several wavelengths between 700 nm and 850 nm are chosen for the large difference in ε between oxyhemoglobin and deoxyhemoglobin. The wavelength at the 810 nm is also chosen for the total hemoglobin concentration, where ε is the same for oxyhemoglobin and deoxyhemoglobin (Murkin & Arango, 2009). Despite of its noninvasiveness and convenience, its applications are still limited. Besides its limited penetration depth to just cortical layer of the brain, it also suffers from drawbacks like poor spatial resolution and inability to distinguish venous and arterial blood.

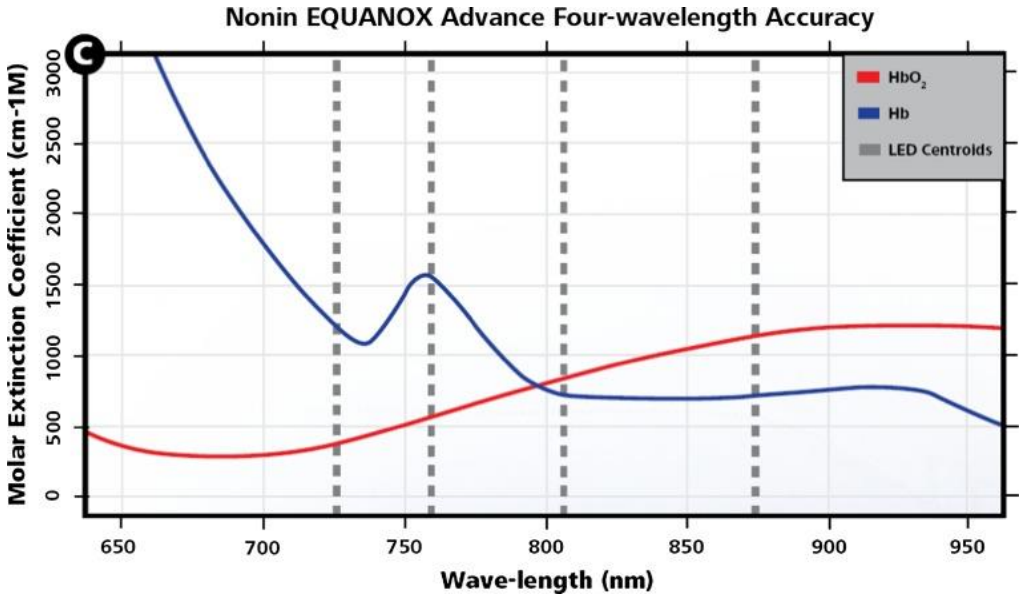

Figure 2-3: The extinction coefficient of oxyhemoglobin (HbO_2) and deoxyhemoglobin (Hb) for light of different wavelengths. The dotted lines present the wavelength of the LED centroids a commercial NIRS uses. The figure is adapted from (Scheeren et al., 2012).

MRI is known for its non-invasiveness and versatile contrast, which could potentially be a good substitute for the two methods mentioned above. More importantly, MRI is sensitive to blood oxygenation. Functional MRI contrast mechanism has been established on the blood oxygenation change induced field change. Different MR properties of blood have been explored in the past 15 years and varieties of techniques have been developed. The regarding techniques can be grouped into four categories: T_2 based method,

susceptibility based method, calibrated BOLD based methods and quantitative BOLD method. I am going to introduce each of them briefly in the following sections.

T_2 based methods

One of the earliest attempts of venous blood oxygenation measurement using MRI was a T_2 based method by Wright et al. (Wright et al., 1991). They measured the T_2 relaxation of the interior vena cava and converted the venous blood T_2 into oxygenation level using an in vitro calibration curve. This method, though conceived more than 20 year ago, composed the general principle of T_2 based venous oxygenation measurement methods: measuring the blood T_2 and then converting the blood T_2 to oxygenation. The blood T_2 is known to have a one to one relationship to its oxygenation, given the hematocrit level. An in vitro calibration curve can be obtained by measuring and fitting the blood sample's T_2 with known hematocrit and oxygenation (Krishnamurthy et al., 2014b; Lu et al., 2012). The in vitro calibration curve is also dependent on field strength and choice of T_2 preparation, i.e. pulses, pulse gap etc.. An example from Lu and colleagues' work is shown in Figure 2-4 (Lu et al., 2012). As shown in Figure 2-4, the blood T_2 increases as the oxygenation level

increases, and decreases with higher hematocrit level. The challenge for this type of method is how to isolate the blood signal and prevent the contamination from the tissue T_2 by partial voluming effect. To overcome this challenge, different techniques have been generated by combining different blood separation techniques with T_2 preparation. I have selected three presentative techniques. Each of them isolates blood signal in a different way and thus has different measurement focus (1D or 2D, large vein or capillaries etc.).

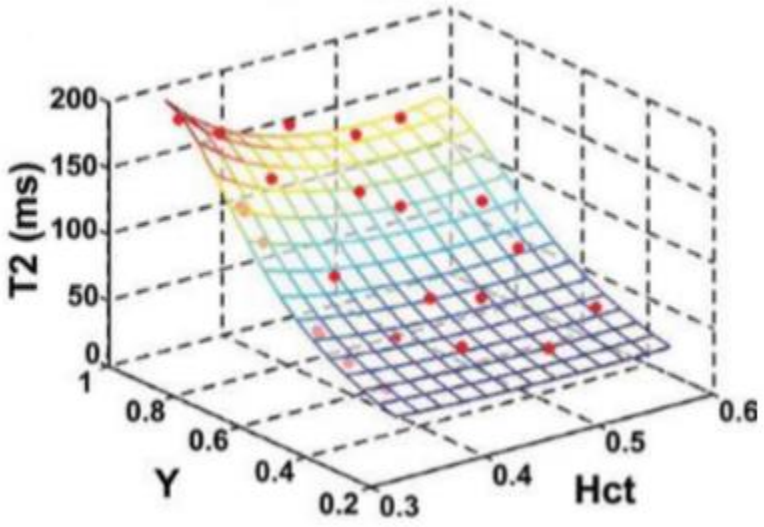

Figure 2-4: The in vitro calibration surface between blood T_2, hematocrit level and oxygenation. The red dots are the experimentally measured data points. The surface is the product of fitting these data points. The figure is adapted from (Lu et al., 2012).

T2-Relaxation-Under-Spin-Contrast (TRUST) is a technique for global venous oxygenation measurement (Lu & Ge, 2008). It employs the spin tagging principle to separate the blood spins from the surrounding tissue spins. Unlike perfusion method arterial spin labeling (ASL), the labeling inversion pulse is applied to the venous side as shown in Figure 2-5. Both the inverted blood spins in the label scan and the uninverted blood spins in the control scan will flow into the imaging slice placed at the posterior superior sagittal sinus. The subtraction of the label and control scan will remove the tissue signal and leave pure blood signal. Different durations of non-selective T_2 preparation will add the blood signal different T_2 weightings. The blood T_2 thus can be yielded through mono-exponential fitting and finally converted into oxygenation level through the calibration plot. Due to the unique signal separation approach, the scope of TRUST has been limited to the single vein per time, making it a global measurement.

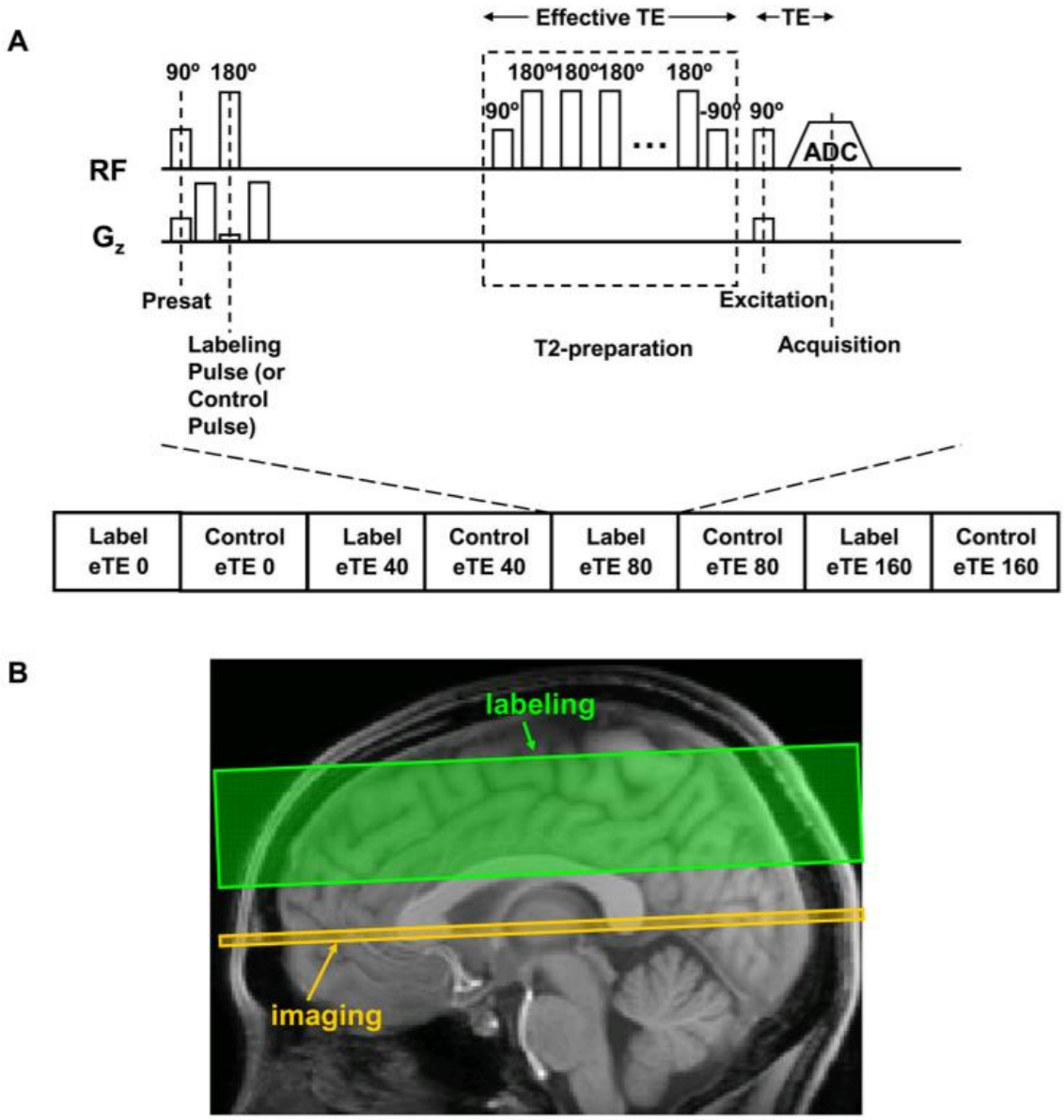

Figure 2-5: The general scheme of TRUST MRI. (A) The TRUST sequence diagram. (B) The positioning of the labeling and imaging slabs. The figure is adapted from (Lu & Ge, 2008).

T_2-Relaxation-Under-Phase-Contrast technique (TRUPC) utilizes phase contrast principle to separate the blood signal based on its velocity, which allows the detection of the oxygenation levels in the veins on a 2D plane (Krishnamurthy et al., 2014a). The sequence diagram is shown in Figure 2-6. The blood spins in the brain are first T_2 prepared and then excited by the excitation pulse, before experiencing one of the bipolar gradients pairs (+ and -). The TRUPC consists of two scans, in which the + and – bipolar gradients are applied separately. As shown in Figure 2-7, the blood spins (blue arrow) will accumulate a phase of φ when experiencing the + bipolar gradients based on its velocity and accumulate a negative phase of –φ when experiencing the – bipolar gradients. The static tissue spins (yellow arrow) will accumulate zero phases in both scans. The complex subtraction of the total signals (dashed black arrow) between the + and – scans will yield a complex difference signal (solid black arrow) only related to the blood signal. Like TRUST, fitting the complex difference signals with different T_2 weightings will allow the estimation of the blood T_2 and eventually the blood oxygenation level. Due to the phase contrast mechanism, this technique is vessel specific, and the slow-flowing venule blood is out of reach for TRUPC.

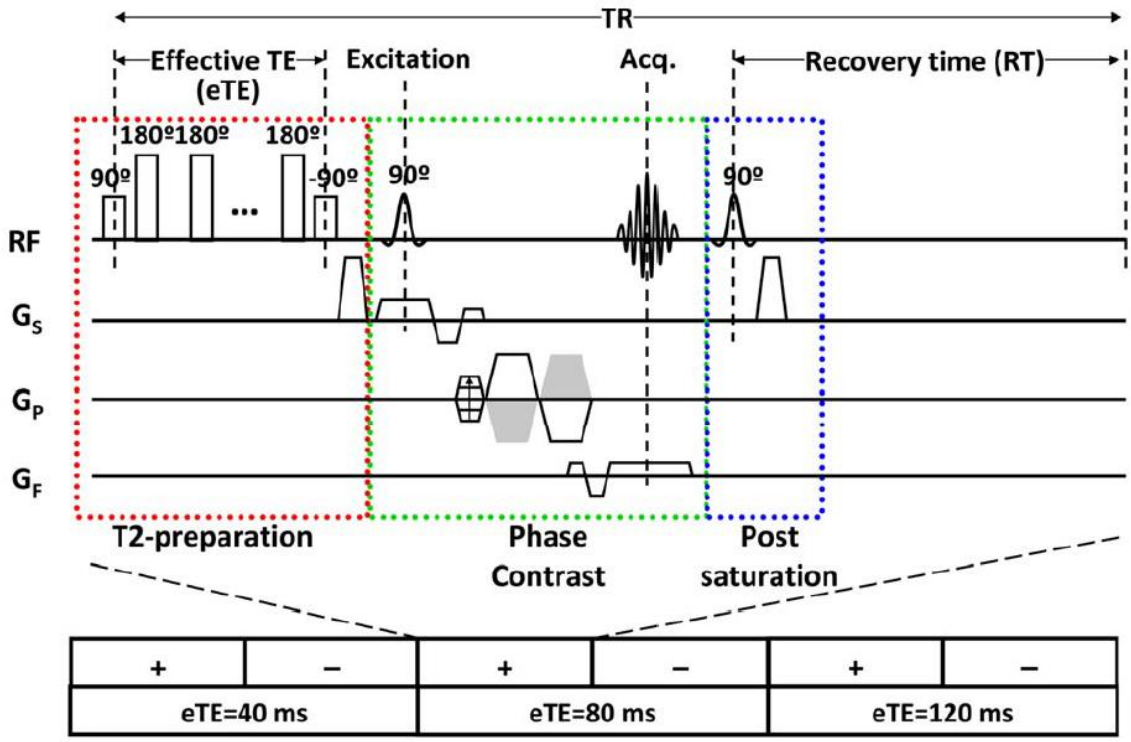

Figure 2-6: The sequence diagram of TRUPC. The figure is adapted from (Krishnamurthy et al., 2014a).

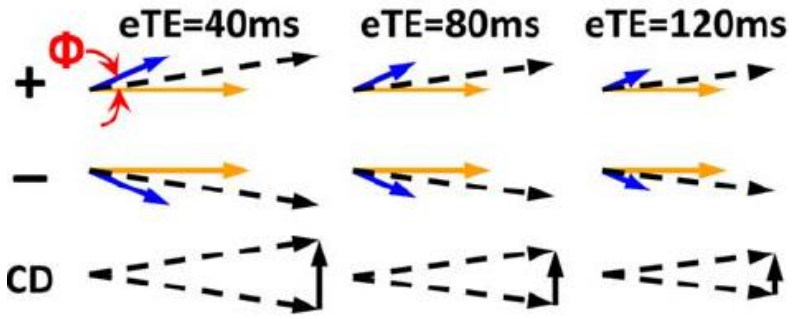

Figure 2-7: The illustration of the mechanism of TRUPC. The figure is adapted from (Krishnamurthy et al., 2014a). Dotted black arrow represents the total

signal, contributed by tissue (yellow arrow) and blood signal (blue arrow). Solid arrow represents the complex difference signal (CD).

Another type of techniques use the velocity selective module to separate the signal of the postcapillary venular blood spins. The first of its kind is named as QUantitative Imaging of eXtraction of Oxygen and Tissue Consumption (QUIXOTIC) method (Bolar et al., 2011). QUIXOTIC applies a velocity selective spin labeling to isolate the venous blood. The sequence diagram is shown in Figure 2-8. The velocity selective (VS) module is a 90^{o}-180^{o}-180^{o}-90^{o} pulse train with gradients inserted between pulses to selectively crush the signal of the fast-flowing species, mostly in large vessels. Control and tag scans are acquired separately by turning the second velocity selective module on and off. According to Figure 2-9, before the first VS module, the spins in all the vessels are relaxed. After the first VS module, all the fast-flowing spins other than the slow flowing spins in the capillary are crushed. The surviving spins keep flowing during the flow out time (TO) and some of them reach the vein. Next, another VS is applied only to the tag scan and kills those spins reached the vein. The subtraction of the label and tag scans will only give the signal from the spins in the venous side. Arterial nulling is used to suppress the fresh spin

flowing into the brain after the first VS module. Guo and Wong later proposed a method named Velocity-Selective Excitation with Arterial Nulling (VSEAN) with a similar idea of velocity selection but using a velocity selective excitation (Guo & Wong, 2012). By applying velocity selective excitation twice, VSEAN selectively excites the spins of the slow flowing blood in the small vessels but not in the tissue. This scheme yields almost twice the signal of QUIXOTIC. Arterial nulling is used to suppress the arterial signal, leaving only the venous signal.

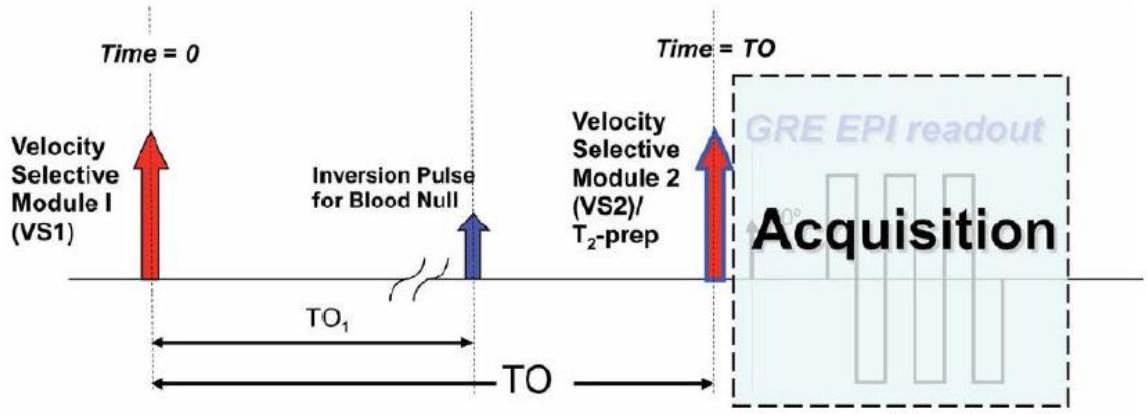

Figure 2-8: The sequence diagram of QUIXOTIC. The figure is adapted from (Bolar et al., 2011).

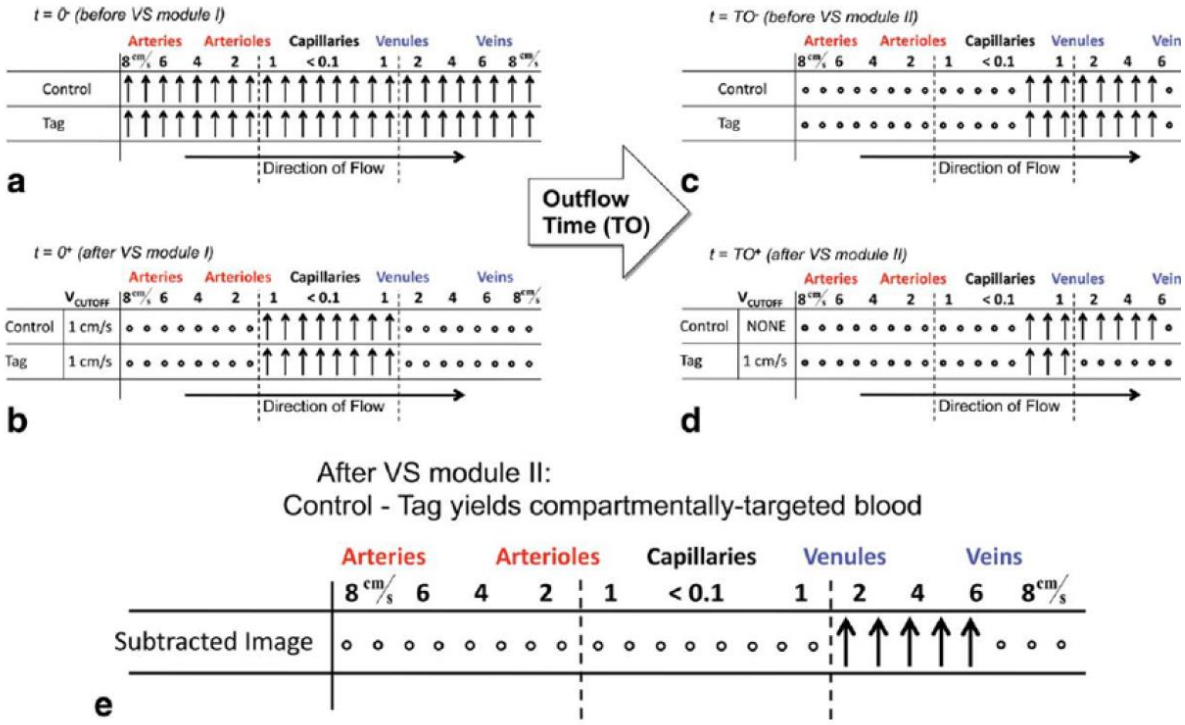

Figure 2-9: The idealized illustration of the venular blood signal isolation process in QUIXOTIC. The figure is adapted from (Bolar et al., 2011). Relaxed and dephased spins are represented by upright arrows and hollow circles, respectively.

Overall, T_2 based methods are one of the more exploited approaches to venous oxygenation measurement by designing delicate pulse sequences. But T_2 based methods may suffer from problems like high energy deposition from the T_2 preparation pulse train, and slow acquisition speed. As a result, the T_2 based methods are currently limited to 2D acquisition.

Susceptibility based methods

There are two aspects of MRI signal: magnitude and phase. While the T_2 based methods measure the magnitude decay of the blood signal, the susceptibility based methods measure the phase change caused by deoxyhemoglobin. Deoxyhemoglobin is strongly paramagnetic and will impose additional magnetic field to the surrounding spins. The blood spins experiencing this additional field will precess at a different frequency and gain a different phase than surrounding tissue spins. For a gradient echo scan of echo time TE, the phase difference $\Delta\varphi$ can be represented as in (Fernandez-Seara et al., 2006):

$$\Delta\varphi = \gamma(B_v - B_s)TE \qquad [2\text{-}1]$$

in which, B_v and B_s is the magnetic field experienced by the spins in the vessel and the surrounding tissues, respectively. γ is the gyromagnetic ratio. To measure the oxygenation in the vein, MR susceptometry studies have modeled the vessel as a cylinder with infinite length. Its oxygenation level can be estimated by:

$$Y_v = 1 - \frac{6\cdot|\Delta\phi|}{\Delta\chi_{do}\cdot Hct\cdot(3cos^2\theta - 1)\cdot(|\gamma B_o|\cdot TE)} \qquad [2\text{-}2]$$

where $\Delta\chi_{do}$ is the susceptibility difference between fully oxygenated and fully deoxygenated red blood cells, Hct is the hematocrit level of the blood. However, the oxygenation measurement needs to know the tilt angle θ to the main field B_0 of the targeted vessels or assume the vessel is parallel to B_0. In the study carried out in (Fernandez-Seara et al., 2006), they took advantage of the orientation of the internal jugular vein and assumed it is parallel to B_0. In another study, when targeting the oxygenation level in the fetal superior sagittal sinus (SSS) using susceptometry, they measured the angle of posterior SSS to the B_0 field in case by case basis, as shown in Figure 2-10 (Neelavalli et al., 2014).

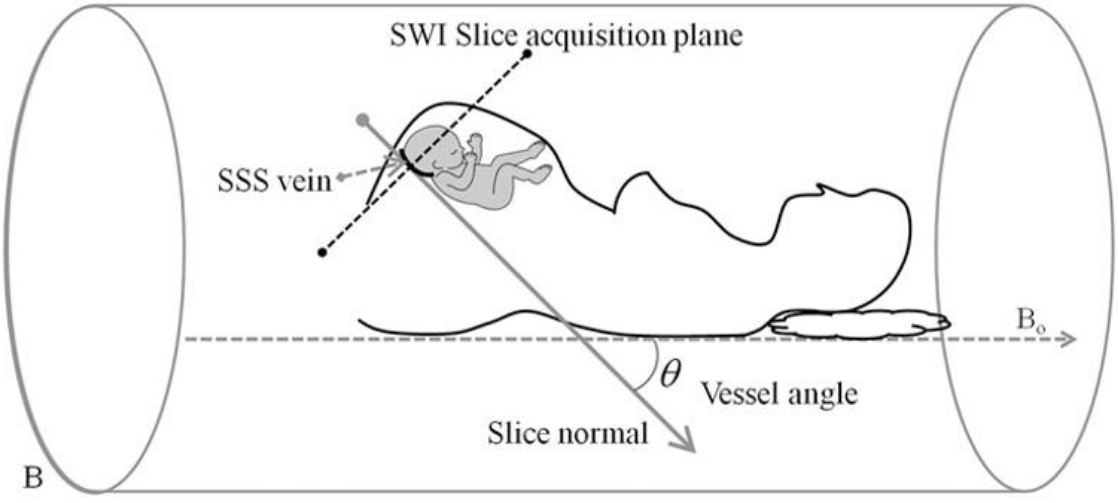

Figure 2-10: Illustration of how the angle of superior sagittal sinus to B_0 is measured by the position information of susceptibility weighted imaging (SWI) slice. The figure is adapted from (Neelavalli et al., 2014).

Even if the vessel angle can be measured, it is still an additional burden, especially when multiple veins need to be measured simultaneously or the vessel trajectory cannot be simply assumed as infinite cylinders. Quantitative susceptibility mapping (QSM) have been proposed to solve the inverse problem, directly mapping the susceptibility in the vessel and then converting it to oxygenation level (Fan et al., 2014). The relationship between the susceptibility and oxygenation level in the vein can be given by:

$$\Delta\chi_{\text{vein}} = \Delta\chi_{do} \cdot (1 - Y_v) \cdot Hct \qquad [2\text{-}3]$$

The converted venous oxygenation map from the susceptibility map is shown in Figure 2-11. However, unlike the T_2 based methods, which aim to separate the blood signal from the surrounding tissue signal, QSM did not apply any signal separation technique and must face the partial voluming effect from the surrounding tissue. It makes the accurate measurement in smaller veins difficult at the current stage.

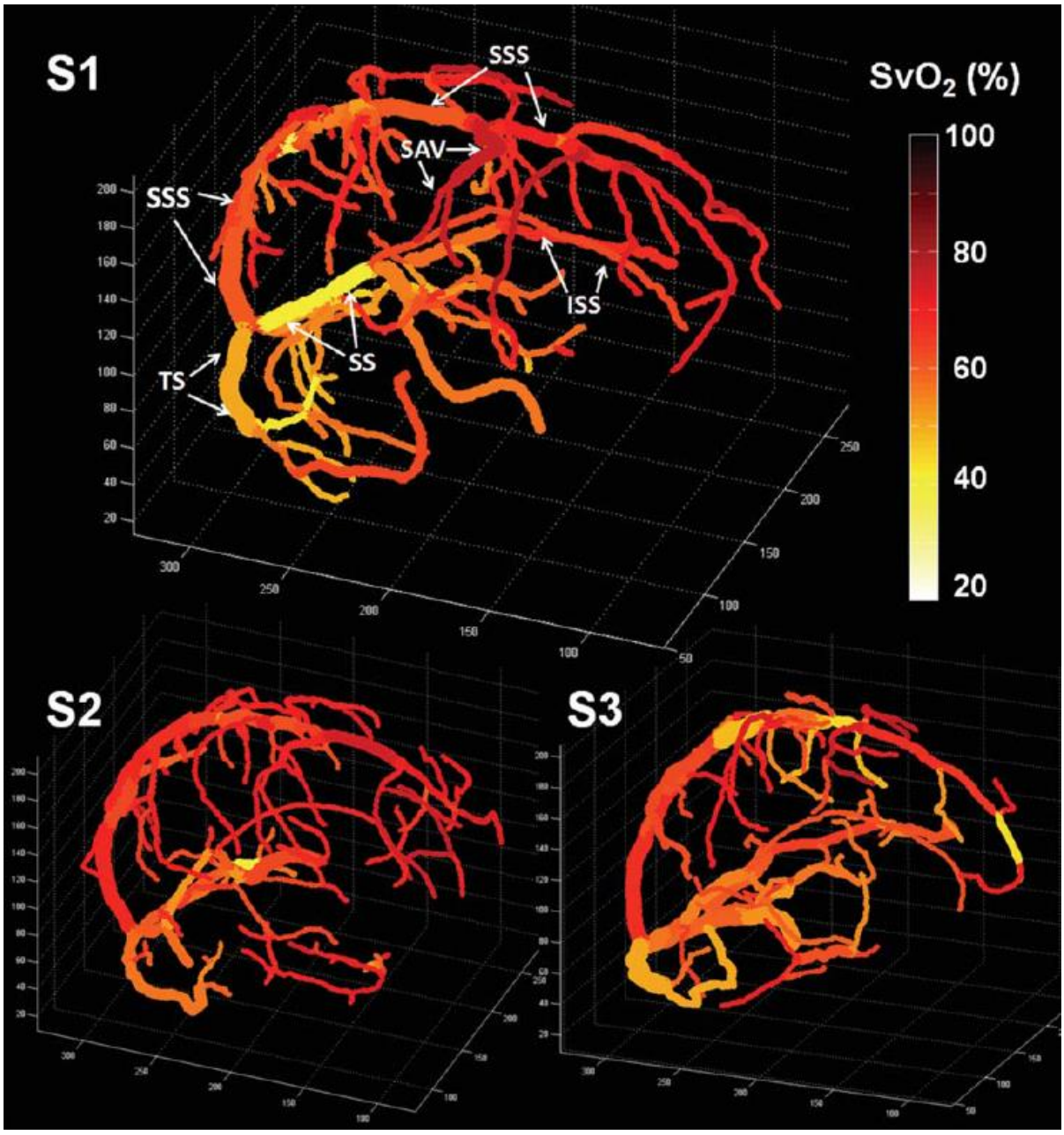

Figure 2-11: Examples of the oxygenation mapped venogram from QSM. The figure is adapted from (Fan et al., 2014).

Calibrated BOLD methods

The third type of method is based on solving of theoretical modeling of BOLD (Bulte et al., 2012; Gauthier & Hoge, 2012; Wise et al., 2013) by modulating the brain states using gas challenges. Hypercapnia and hyperoxia challenges are conducted along with BOLD and ASL scan in this method. These challenges can induce BOLD signal change as well as CBF change. So the venous oxygenation can be solved by incorporating additional conditions provided for the BOLD model. The details of the model are described below according to (Wise et al., 2013).

According to the Hoge and Davis model (Davis et al., 1998; Hoge et al., 1999), the BOLD signal can be modeled as:

$$\frac{\Delta S}{S_0} = M[1 - \left(\frac{CBF}{CBF_0}\right)^{\alpha} \left(\frac{[dHb]}{[dHb]_0}\right)^{\beta}] \quad [2\text{-}4]$$

in which $\Delta S/S_0$ is the fractional BOLD signal change, [dHb] and CBF are referring to the changed state, and $[dHb]_0$ and CBF_0 are referring to baseline state deoxyhemoglobin and cerebral blood flow. β is the length scale of the vessel and is different for large and small vessels (Gauthier & Hoge, 2012). M is the upper limit of BOLD signal change defined by completely removal of deoxyhemoglobin in the voxel:

$$M = TE \cdot A \cdot CBV_0 \cdot [dHb]_0^{\beta} \quad [2\text{-}5]$$

A is a constant based on the B_0 strength and vessel geometry. CBV_0 is the baseline cerebral blood volume. The CBF change can be substituted by the CBV change by the relationship established in (Grubb et al., 1974):

$$(\frac{CBV}{CBV_0}) = (\frac{CBF}{CBF_0})^{\alpha} \quad [2\text{-}6]$$

α is the Grubb coefficient (Grubb et al., 1974).

On the other hand, the cerebral metabolism rate of oxygen ($CMRO_2$) based on Fick principle can be calculated as:

$$CMRO_2 = (Y_a - Y_v) \cdot CBF \quad [2\text{-}7]$$

in which Y_a and Y_v are the arterial and venous oxygenation, respectively. I can further assume the different states of the brain during the gas challenge do not alter the $CMRO_2$.

$$(Y_a\ |_0 - Y_v\ |_0) \cdot CBF_0 = (Y_a - Y_v) \cdot CBF \quad [2\text{-}8]$$

By interpreting the Y_v as a function of deoxyhemoglobin concentration [dHb] and oxyhemoglobin concentration [Hb]:

$$\frac{[dHb]}{[dHb]_0} = \frac{CBF_0}{CBF} - \frac{1}{[dHb]_0}\{\frac{1}{\phi}(CaO_2 - (\frac{CBF_0}{CBF})CaO_2\ |_0) + [Hb](\frac{CBF_0}{CBF} - 1)\} \quad [2\text{-}9]$$

Combining equation 2-4, 2-5 and 2-9, $[dHb]_0$ can be solved by feeding the BOLD and CBF information from different brain states in the gas challenge, which is related to the venous oxygenation level:

$$[dHb] = [Hb](1 - Y_v) \quad [2\text{-}10]$$

The advantages of these methods are the simple acquisition method and based on the straightforward and well-established BOLD model. Full brain coverage and regional venous oxygenation information is also advantageous. While the gas challenges may not be hard to perform, the assumption that the gas modulation is iso-metabolic may not held true for both hypercapnia challenge (Xu et al., 2011) and hyperoxia challenge (Xu et al., 2012). The use of a true iso-metabolic gas challenge can help with the perfection of these methods (Peng et al., 2017).

Quantitative BOLD method

Quantitative BOLD (qBOLD) was first proposed by He and Yablonskiy in 2007 (He & Yablonskiy, 2007). The qBOLD method is based on the modeling of gradient-echo signal decay behavior. It attributes the gradient echo signal decay to three regimes: macroscopic effects, mesoscopic effects, and microscopic effects. The microscopic effects are caused by spin-spin relaxation

and diffusion of spins, or commonly known as T_2 relaxation, which cannot be refocused. The macroscopic effects are from the imperfect shimming of the B_0 field, at the scales of at least multiple voxels. The mesoscopic effects are in between, scale wise, from the field inhomogeneity caused by the vessel containing deoxygenated hemoglobin. Both mesoscopic and macroscopic effects can be refocused by 180^o refocusing pulse. The mesoscopic effects are particularly interesting because it is related to the venous oxygenation.

An oversimplified qBOLD model was adapted from (Blockley et al., 2015), to illustrate the essence of the qBOLD idea here. This model only considers a single tissue type with no intravascular contribution. According to (Yablonskiy & Haacke, 1994), the behavior of the spin echo signal can be divided into two time scales: long and short. The long and short scales can be determined by the characteristic time, t_c. As shown in Figure 2-12, the time from TE-1.5t_c to TE+1.5t_c falls in the short time scale, in which the signal decay is quadratically exponential. The long-time scale is the time interval A and B, which is before and after the short time interval, respectively. During the long time interval, the signal can be modeled for interval A and B, respectively:

$$\ln\big(S(t)\big) = c_A - (R_2 - R_2')(t - TE) - a_A(t - TE)^2 \qquad [2\text{-}11]$$

$$\ln\big(S(t)\big) = c_B - (R_2 + R_2')(t - TE) - a_B(t - TE)^2 \qquad [2\text{-}12]$$

The venous volume (V in the Figure 2-12) is related to the difference between the fitted S_0, denoted as $S_{fit}(TE)$ here and measured signal at TE, $S_{meas}(TE)$:

$$V = \ln\left(S_{fit}(TE)\right) - \ln\left(S_{meas}(TE)\right) \quad [2\text{-}13]$$

in which $S_{fit}(TE)$ is the average of intercepts c_A and c_B. The deoxyhemoglobin concentration [dHb] can be calculated as:

$$[dHb] = \frac{3}{4}\frac{R_2}{\pi \cdot \omega_0 \cdot V \cdot \Delta\chi} \quad [2\text{-}14]$$

where $\Delta\chi$ is the susceptibility difference between fully deoxygenated and fully oxygenated red blood cell, and ω_0 is the Larmor frequency.

Experimentally, qBOLD uses gradient-echo sampling of spin-echo (GESSE) method to catch the signal evolution densely for the later fitting. A single k-line is acquired in each echo for each shot (data points in Figure 2-12). The sequence is repeated to acquire the whole k-space.

Things are much more complicated in the reality. The contributions of signal from the intracellular space (grey and white matter), extracellular space (cerebrospinal fluid) and intravascular space are all modeled individually and fitted together. Extra care should be given in the selection of the starting point in the multi-parameter fitting.

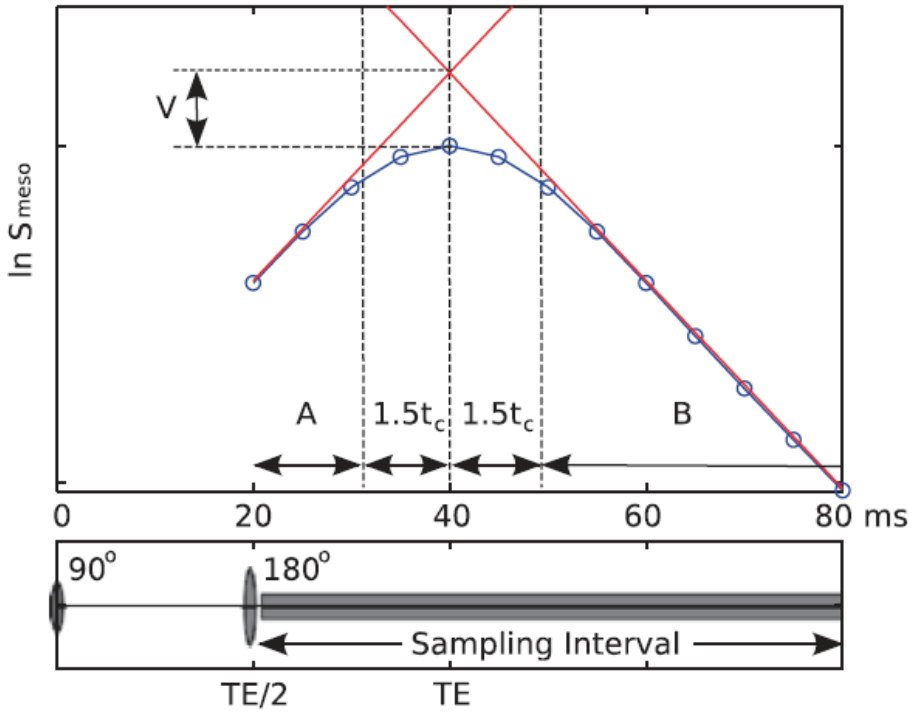

Figure 2-12: Illustration of signal decay from mesoscopic effects (circles) during the signal evolution in spin echo. The long time intervals in straight lines are extrapolated to the echo time TE (red lines). The figure is adapted from (Blockley et al., 2015).

R_1 based method

While it is well known that BOLD imaging relies on the change of transverse relaxation mainly due to change of deoxyhemoglobin concentration, the longitudinal relaxation is also related to the oxygen level in tissue. R_1 has

been found to increase with the increase in the concentration of the dissolved paramagnetic O_2 molecules in the blood or tissue. This effect from the O_2 molecules is known as Tissue Oxygen Level Dependent imaging (TOLD) (Matsumoto et al., 2006). The acquisition of TOLD imaging is usually T_1 weighted gradient echo or T_1 mapping using inversion recovery sequences to capture the T_1 related signal change. Since TOLD uses O_2 molecule as contrast agent, TOLD imaging is often performed with high oxygen content gas challenge. For example, Hallac et al., have reported that the TOLD signal increase upon hyperoxia or carbogen challenge in smaller tumor is higher than the signal increase in larger tumor due to less hypoxia the small tumor experiences (Hallac et al., 2014). The TOLD effect has also been found to be associated with the absolute pO_2 and radiation response in the tissue in the same study. The TOLD imaging has provided a different perspective since it is directly related to the concentration of O_2 as opposed to the concentration of deoxyhemoglobin in BOLD imaging. These two effects can be complimentary for the understanding of the pathology in diseases, especially the ones cause change in oxygenation metabolism. Techniques assessing both BOLD and TOLD effects simultaneously are of particular interest (Ding et al., 2013; Remmele et al., 2013).

Conclusion

In this chapter, different techniques measuring cerebral venous oxygenation are briefly reviewed. The methods before MRI are more well-established than the MRI methods, but each has its own disadvantages preventing its growth. The MRI methods has shown some promises in the field especially for its noninvasiveness, but need to be further refined technical wise and eventually available in clinical settings.

CHAPTER THREE

Cerebral venous oxygenation in hypertension

Introduction

About one out of three adults in the United States has hypertension (Nwankwo et al., 2013). Hypertension is one of the most important risk factors to cardiovascular disease, which is among the top 5 causes of the death in the United States, according to most recent data from CDC (Heron, 2016). Hypertension has also been identified as a major vascular contributor to dementia (Gasecki et al., 2013; Gorelick et al., 2011). The theory has been formed that the hypoperfusion caused by hypertension will disrupt the oxygenation delivery to the brain tissue and the resultant brain hypoxia-ischemia will further increase the brain's amyloid-β burden and promote dementia (Iadecola & Davisson, 2008).

Hypertension thickens and stiffens the arterial vessel walls and reduces the lumen of the arteries, which hinders the normal perfusion (Baumbach & Heistad, 1988). This reduction in CBF can affect different regions in the brain in a heterogeneous manner (Alosco et al., 2014; Beason-Held et al., 2007;

Muller et al., 2012). The similar fashion was also found in the reduction of the cortical volume during hypertension (Alosco et al., 2014; Raz, 2005). But the reduction in venous oxygenation, which is often considered as the direct consequence of hypoperfusion, has not been widely explored, especially on the regional basis. While the global increase in oxygen extraction fraction has been observed in the hypertensive patients previously (Fujishima et al., 1995; Hafkenschiel et al., 1954; Yao et al., 1992), only one study has reported the positive correlation between blood pressure and OEF in thalamus using PET (Fujishima et al., 1995). The evidence for the regional variation of venous oxygenation in the hypertension induced brain hypoxia-ischemia is still lacking. One of the possible reasons could be the shortage of a simple and non-invasive method to measure regional cerebral venous oxygenation in the past. The cerebral venous oxygenation measurement used to be dominated by ^{15}O-PET (Ibaraki et al., 2008), which requires complicated procedures, such as on-site cyclotron, inhalation of radioactive gas and arterial blood sampling. In the past decade, several MRI techniques have emerged in this field. My lab has developed a technique named T_2-Relaxation-Under-Phase-Contrast (Krishnamurthy et al., 2014a), which can measure the oxygenation level in large cerebral veins, such as superior sagittal sinus (SSS) and internal cerebral

veins (ICV). TRUPC exploits the phase contrast principle to separate the pure blood signal from the static tissue. Then the blood signal has gone through different durations of T_2 preparation, allowing the T_2 measurement of blood. The blood T_2 can be converted in oxygenation through an in vitro calibration curve (Lu et al., 2012).

In the present study, by applying the TRUPC techniques to a cohort from Dallas Heart Study to measure the regional venous oxygenation in SSS and ICV, I assessed the relationship between blood pressure and regional venous oxygenation. I also test if the regional venous oxygenation is related to morphological change, as in regional brain volumes.

Methods

Participants and Experimental procedure

Participants were recruited from the cohort of Dallas Heart Study, a large scale multi-ethnic probability-based study. The study protocol was approved by the university Institutional Review Board, and written informed consent was obtained from all participants. The details of DHS were described previously in (Victor et al., 2004). All of the participants underwent a MRI experiment consisted of a TRUPC and a T_1 anatomical scan in a Philips 3T Achieva MRI

scanner (Philips Healthcare, Best, The Netherlands). Their blood pressure was measured three times at different time points of the experiment: before, after and during the break of the MRI experiment. The average of the three measurements was used in the subsequent study. A patient is considered as hypertensive either if his systolic blood pressure is over 139 mmHg or his diastolic blood pressure is over 89 mm Hg (Chobanian et al., 2003). Thus, the subjects can be categorized into 30 hypertensive patients (18F) and 36 healthy controls (15F). All the patients meet the systolic blood pressure standard and 9 patients meet the diastolic blood pressure standard. Their average age was 68±5.1 years and 67.1±5.1 years for patient and control groups, respectively. The average systolic and diastolic pressure was 156±15 mmHg and 86±8 mmHg for hypertension group, 129±7 mmHg and 76±6 mmHg for control group.

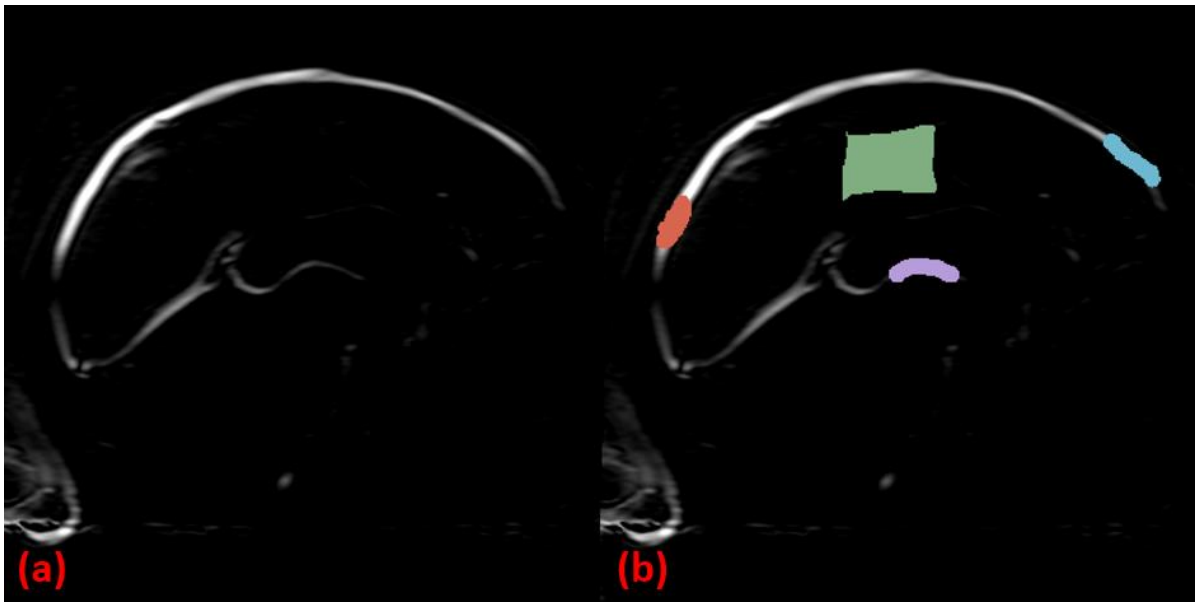

Figure 3-1: Complex difference image from TRUPC with and without ROI overlaid. (a) Example of the complex difference image from 0 ms eTE. (b) Four manually drawn ROIs were overlaid on (a). Color coding for each ROI is as follows: anterior SSS in blue, posterior SSS in red, ICV in purple and non vessel region in green for noise determination.

The TRUPC was a 2D single slice scan positioned on the mid sagittal plane of the brain as shown in Figure 3-1a. The vessels of interest, superior sagittal sinus and internal cerebral veins can be sampled at the same time in the mid sagittal slice. The imaging parameters were as follows: gradient echo readout, FOV=200×200 mm^2, acquisition matrix=276×83, voxel size=0.72×2.41 mm^2, slice thickness=5 mm, V_{enc}=15 cm/s in anterior-posterior

direction, flip angle/TE/ΔTE/TR= 90º/4.3 ms/571 ms; T_2-preparation module used composite block pulses with MLEV-16 phase cycling scheme; three effective TE (0 ms, 40 ms and 80 ms) weighted sets of images were acquired. The scan duration was 5.5 min. A T_1 weighted Magnetization-Prepared Rapid Gradient-Echo (MPRAGE) was also performed for the brain volume quantification. The imaging parameters were as follows: 3D gradient echo readout, sagittal slice orientation, FOV=260×155×240 mm^3, acquisition matrix=260×137×240, voxel size=1×1.13×1 mm^3, flip angle/TE/TR=12º/3.5 ms/9.6 ms, Sensitivity encoding (SENSE) factor=2, scan duration=3.5 min.

Data Analysis

To quantify the venous oxygenation from TRUPC, an ROI approach was adopted. The complex difference images were first realigned by FMRIB Software Library to the 0 ms eTE image. Three vessel ROIs were drawn manually on the 0 ms eTE complex difference images for anterior (blue) and posterior (red) parts of superior sagittal sinus and internal cerebral veins (purple) for each subject, as shown in Figure 3-2b. An additional ROI (green) was on the non-vessel region to determine the noise level. The manual ROI was further trimmed by thresholding at 2 times of the mean noise level sampled in

the non-vessel ROI in each eTE image. The final ROI was the product of AND operation of the trimmed ROIs from each eTE image. The signal intensity in each ROI was averaged for each eTE and was fitted monoexponentially for its T_2 relaxation time. The T_2 relaxation was further converted into oxygenation value using an in vitro T_2-Y_v calibration plot from our lab (Lu et al., 2012). The fitting parameter dR_2 was used for quality control. If the fitting process yielded a ΔR_2 bigger than 5 Hz, the data were excluded for poor fitting reliability reason. The hematocrit level was assumed 0.40 for female and 0.42 for male.

The T_1 images were fed to MRI cloud (http://mricloud.org) for segmentation and volume quantification (Mori et al., 2016). MRI cloud offers a fully automated cloud service for T_1 based brain parcellation. The level 4 of the default template, Adult_286labels_1oatlases_V5L was used, which divides the brain in 135 cortical and subcortical regions. The regions that are drained by anterior SSS and ICV were selected and listed in Table 3-1. The volume from the left and right of the same regions were combined for each subject to reduce number of comparisons.

Regions drained by anterior SSS	Regions drained by ICV
Superior frontal gyrus	Hippocampus
Middle frontal gyrus	Caudate
Inferior frontal gyrus	Putamen
Orbital gyrus	Globus pallidus
	Thalamus

Table 3-1: The brain regions drained by anterior SSS and ICV. The volume of each region was quantified in each subject.

The image processing and statistical analysis was done by inhouse Matlab scripts. For systolic blood pressure, a multiple regression analysis was employed with regional venous oxygenation in anterior SSS and ICV. Similar analysis was also done using the relative venous oxygenation, which is the venous oxygenation in the anterior SSS and ICV subtracted by the venous oxygenation in the posterior SSS. The oxygenation in posterior SSS has been shown to be similar to the oxygenation in the internal jugular vein and can be used as an approximation to global venous oxygenation in the brain (Xu et al., 2009). Furthermore, for individual relative venous oxygenation, multiple regression analysis was employed with the volumes of each brain region

drained by this vessel as the dependent variable, as denoted in Table 3-1. Age and gender were always included as the independent variables in all the regression analysis. The p values are from two-tail t-test.

Results

The average oxygenation levels in anterior SSS, posterior SSS and ICV are 0.63±0.06, 0.61±0.06 and 0.60±0.10, respectively. All of them fall into the physiological venous oxygenation range in the brain. Figure 3-2 shows the scatter plot between the systolic pressure and the regional oxygenation of anterior SSS and ICV. No significant correlation was found in either one (p=0.68 for anterior SSS and p=0.31 for ICV, N=63).

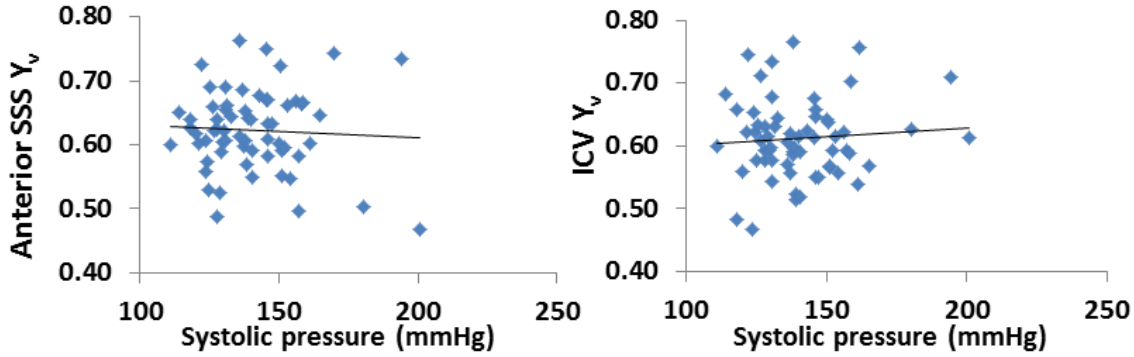

Figure 3-2: The scatter plot between the anterior SSS (left, N=63) and ICV (right, N=63) oxygenations and the systolic pressure. The lines are linear

fittings of Y_v and blood pressure data. Regression analysis showed that the relationship between the regional oxygenation and the systolic pressure was not significant in anterior SSS ($p=0.68$) and ICV ($p=0.31$)

The similar relationship was also tested using the relative venous oxygenation instead of the venous oxygenation for the same regions. The relative regional oxygenation is the regional venous oxygenation from anterior SSS or ICV subtracted by the venous oxygenation in the posterior SSS in each subject. Figure 3-3 shows the scatter plot between the relative oxygenation in anterior SSS and ICV and the systolic pressure. The systolic pressure was found to be significantly correlated with the relative venous oxygenation in anterior SSS ($p<0.05$, $N=63$) at rate of 1.2×10^{-3} per mmHg. A trend of decline was also found between the relative venous oxygenation in ICV and the systolic pressure at a similar rate of 9.5×10^{-4} per mmHg ($p=0.06$, $N=63$).

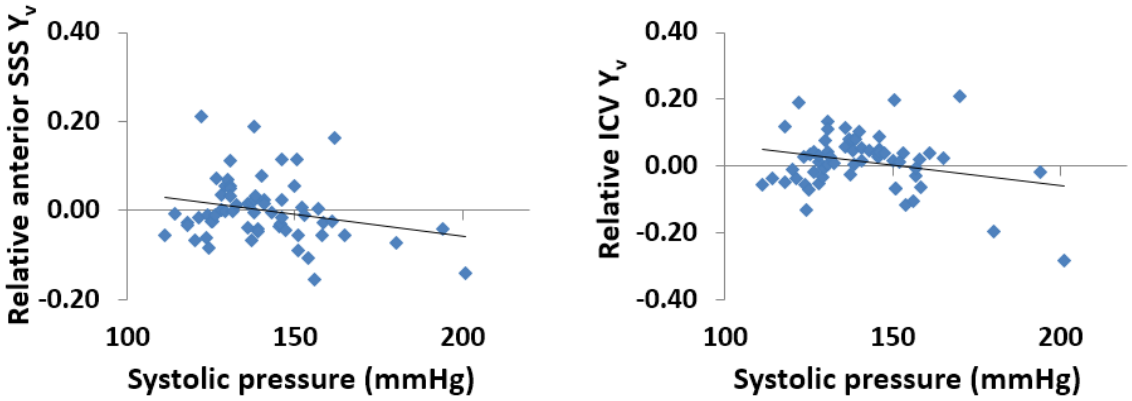

Figure 3-3: The scatter plot between the relative venous oxygenation in anterior SSS (left, N=63) and ICV (right, N=63) and the systolic pressure. The lines are linear fittings of the relative Y_v and blood pressure data. Regression analysis showed that the relationship between the relative venous oxygenation and the systolic pressure was significant in anterior SSS ($p<0.05$) and marginally significant in ICV ($p=0.06$)

The hypertensive group and control group are looked at separately. Figure 3-4 is the scatter plot between relative anterior SSS oxygenation and systolic pressure in these two groups. The significant negative correlation found in Figure 3-4 was consistent with the findings in Figure 3-5 but at a higher rate of 3.4×10^{-3} per mmHg for hypertensive group ($p<0.01$, N=29). The correlation was not observed in the control group ($p=0.53$, N=34), however.

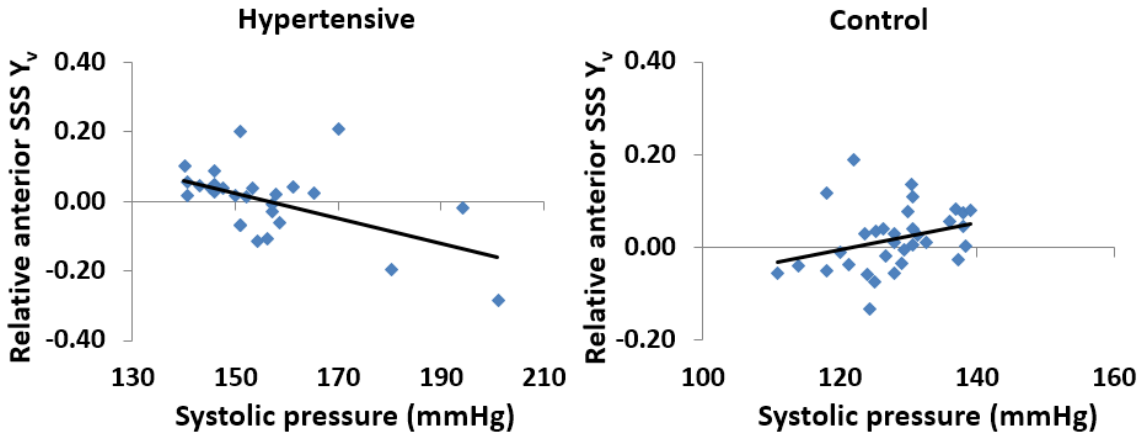

Figure 3-4: The scatter plot between the relative anterior SSS oxygenation and systolic pressure in hypertensive group (left) and control group (right). The lines are linear fittings of the relative Y_v and blood pressure data. The relationship was significant in hypertensive group ($p<0.01$, $N=29$) but not in control group ($p=0.53$, $N=34$).

A significant negative correlation was also observed between the relative ICV oxygenation and systolic pressure in the hypertensive group ($p<0.05$, $N=27$) at rate of 2.2×10^{-3} per mmHg, as shown in Figure 3-5. No such correlation was shown in the control group ($p=0.36$, $N=36$).

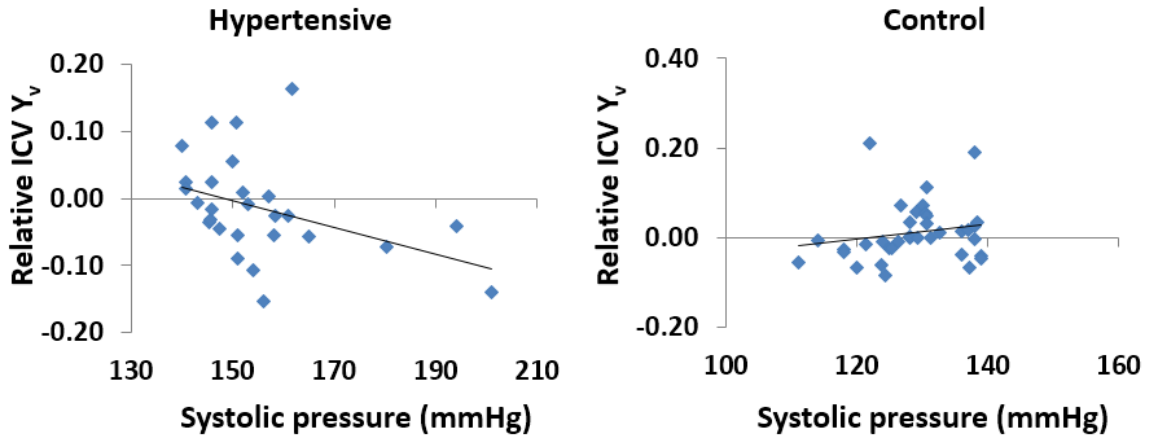

Figure 3-5: The scatter plot between the relative ICV oxygenation and the systolic pressure in hypertensive group (left) and control group (right). The lines are linear fittings of the relative Y_v and blood pressure data. The relationship was significant in hypertensive group ($p<0.05$, $N=27$), but not in control group ($p=0.36$, $N=36$).

No significant correlation was found in the relationship between the anterior SSS oxygenation and the volumes of front lobe regions. However, as shown in Figure 3-6, the relative ICV oxygenation was positively correlated with the hippocampus (HC) volume at the rate of 2730 mm^3 ($p<0.05$. $N=63$). There was also a positive trend between the relative ICV oxygenation and the thalamus (TL) volume at the rate of 2586 mm^3 ($p=0.06$, $N=63$). The age effect was significant in both cases with $p<0.05$.

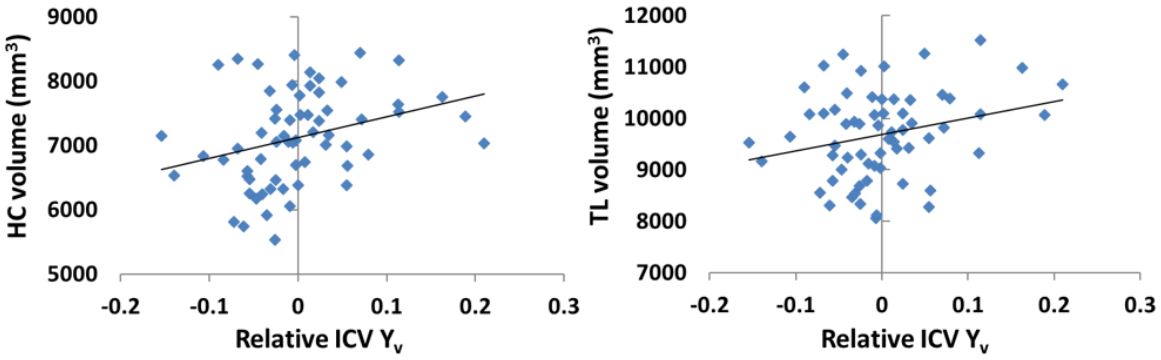

Figure 3-6: The scatter plot between the relative ICV oxygenation, and the hippocampus (HC) volume (left) and the thalamus (TL) volume (right). The line is a linear fitting of the relative Y_v and blood pressure data. The linear relationship of the relative ICV oxygenation was significant with the HC volume ($p<0.05$, $N=63$) and marginally significant with the TL volume ($p=0.06$, $N=63$).

Discussion

In the present study, I have employed a MRI venous oxygenation measurement technique, TRUPC to study the effect of hypertension to regional venous oxygenation. The study has revealed that the venous oxygenation tends to be lower in the frontal lobe and deep brain comparing to the rest of the brain,

when systolic pressure is high. This association was led by the hypertensive group. It was also found that the smaller volume of the hippocampus and thalamus has also been associated with the lower regional venous oxygenation in such regions.

The study is the first of its kind applying MRI to look at the regional venous oxygenation in hypertension. The design of the study has utilized the advantage of the vessel specific oxygenation mapping method, TRUPC. The anterior part of SSS and ICV contain venous blood directly drained from the frontal cortex and deep brain, respectively, before mixing with the blood drained from other regions. The TRUPC positioning on the mid sagittal plane of the brain therefore can measure them all in a single scan. Thus it allows studying of venous oxygenation in these regions specifically. It is known that the baseline global cerebral venous oxygenation level varies widely from 0.4 to 0.8, even in heathy groups (Lu et al., 2011). The introduction of the relative venous oxygenation concept has removed the effect from the variation of baseline global venous oxygenation, and focused on the regional difference in venous oxygenation. The posterior SSS oxygenation used in the normalization has been proven to be a good substitute to global venous oxygenation, which is sampled in the internal jugular vein (Xu et al., 2009).

Our findings can be explained with regional CBF change associated with hypertension. The reduction of CBF in hypertensive patients has been reported to be most predominate in the frontal cortex and temporal lobe (Alosco et al., 2013; Beason-Held et al., 2007), which contains structures drained by anterior SSS and ICV. To keep up with the metabolic level during the hypoperfusion, these brain regions need to extract more oxygen from the same amount of blood, causing chronic hypoxia in the tissue (Aliev et al., 2003).

Our findings are also consistent with the previous studies on the cortical volume in hypertensive patients. The hypertension is widely associated with total brain volume reduction in previous studies (Beauchet et al., 2013; DeCarli et al., 1999; Swan et al., 1998) and was shown to have regional specificity (Raz et al., 2003). Hippocampal and prefrontal atrophy has been widely reported to be associated with hypertension (Beauchet et al., 2013; Raz, 2005; Raz et al., 2003; Raz et al., 2007). For example, Raz et al. has reported that hypertension have been identified as a negative modifier in cortical volume during aging and selectively targeted at prefrontal cortex and hippocampus (Raz, 2005; Raz et al., 2003). This targeted effect on prefrontal cortex further influenced the cognitive function in hypertension patients (Raz et al., 2003). The volume of thalamus was also reported to be smaller in hypertensive population (Strassburger et al.,

1997). The results presented here could provide more insights in the mechanism of such changes from the perspective of oxygen metabolism.

The results of the study need to be interpreted in the context of a few limitations. First, the medication usage and medical history of the participants are not considered in the study. This could induce noise to the study, especially to analysis of the anatomical volume, for its longitudinal effect. For example, a patient with prolonged hypertension history but was under hypertension treatment at the time of the measurement, may be categorized in the control group with low pressure blood. But according to the indication of the study, he would likely have a lower regional brain volume.

Another limitation is from the technique used. The TRUPC applied in this study is a 2D technique for large vessels. This limited the scope of the study to part of the frontal lobe and deep brain regions. The drainage of the upper stream of the veins is assumed be region specific. But, strictly speaking, the upper stream blood in these large veins is already a mixture of the venous blood from different regions, which could reduce the detection power of the method. Additionally, the regions of interest may not always align in a 2D plane due the anatomical variations, TRUPC failed to capture the anterior SSS or ICV in about 10% of the subjects. A 3D technique is desired to look at specific

draining veins for each region. Inspired by this study, I have developed a novel 3D oximetry, which will be discussed in details in the next chapter.

Finally, the conversion from T_2 to venous oxygenation requires the knowledge of hematocrit level. The hematocrit level can change under pathological conditions. It has been found that the hypertensive patients have a slightly but significantly higher hematocrit level by about one unit than the control group (Cirillo et al., 1992; Tarazi et al., 1966). The study in the future should take this potential difference in mind and measure the individual hematocrit for more accurate oxygenation measurement.

Conclusion

I have applied a noninvasive 2D MRI technique, TRUPC to assess the effect of hypertension to regional venous oxygenation in the brain. The lower venous oxygenation in the frontal lobe and deep brain are associated with high systolic pressure. In addition, the volume reduction in hippocampus and thalamus is correlated with the decreased venous oxygenation in these regions. Imaging marker Y_v reported here may prove valuable in understanding of hypoxia, CBF and cortical volume reduction in these regions caused by the hypertension. However, the 2D scope of the TRUPC has limited its potential in

assessing the venous oxygenation at more cortical locations and at more precise manner. This limitation has inspired me to develop a 3D oximetry in brain in the next chapter.

CHAPTER FOUR

Three-dimensional mapping of brain venous oxygenation using R_2^* oximetry

Introduction

Cerebral venous oxygenation (Y_v) is closely associated with the brain's oxygen extraction, metabolism, and to some extent neural activity, and is a promising biomarker in several major neurological diseases including stroke (Derdeyn et al., 2001; Gupta et al., 2014), tumor (Leenders, 1994) and Alzheimer's disease (Ishii et al., 1996; Nagata et al., 2000; Thomas et al., 2016). However, measurement of cerebral venous oxygenation in humans has proven difficult. ^{15}O positron emission tomography (PET) was one of the first methods developed to measure Y_v, but this method requires inhalation of radioactive gas, arterial blood sampling, and an onsite cyclotron to produce the short half-life ^{15}O tracer (Mintun et al., 1984). As a result, only a small number of laboratories are still performing such experiments in recent years.

An active research topic in the MRI field is, therefore, the development of new techniques to non-invasively measure Y_v in humans. To this end,

measurement of global, whole-brain venous oxygenation is now relatively well-established. One can either use the T_2-Relaxation-Under-Spin-Tagging (TRUST) (Lu & Ge, 2008) or phase susceptometry method (Fernandez-Seara et al., 2006) to determine global cerebral Y_v within approximately one minute. In contrast, considerable technical development is still needed for MRI techniques of regional Y_v quantification, which would have a greater potential for clinical applications. While all such techniques are based on the paramagnetic property of deoxyhemoglobin, different types of methods have focused on magnitude (Gauthier & Hoge, 2012; He & Yablonskiy, 2007; Wise et al., 2013) or phase (Fan et al., 2014; Xu et al., 2014) manifestations of these effects. One particular line of techniques is based on a calibratable relationship between blood R_2^* (or R_2^*) and oxygenation (Y) (Chen & Pike, 2009; Lu et al., 2012; Zhao et al., 2007). By designing advanced MR pulse sequences to accurately measure blood transverse relaxation in vivo, one can obtain a quantitative assessment of cerebral oxygenation without using any contrast agent or physiological challenge. Although several efforts have demonstrated promising results (Bolar et al., 2011; Guo & Wong, 2012; Krishnamurthy et al., 2014a), the spatial coverage of these prior works has been limited to a single slice. Therefore, in

order to have a practical utility in clinical settings, expansion of these techniques to 3D, ideally with whole-brain coverage, is highly desirable.

The goal of this study is to develop 3D acquisition and analysis schemes to measure blood oxygenation in human cerebral veins after accounting for partial voluming between blood and tissue. The proposed method employs velocity-encoded phase contrast imaging to differentiate flowing blood signal from static tissue, and applies flow-compensated multi-gradient-echo acquisition to rapidly map blood R_2^*. In vivo experiments were performed to demonstrate the feasibility and reproducibility of this method. Sensitivity of the method to known effect of oxygenation change was tested by hyperoxia physiological challenge. In vitro experiments were performed to establish the R_2^*-Y calibration plot, from which the in vivo R_2^* values could be converted to physiological value of venous oxygen saturation fraction. Validation was performed by comparing the Y_v measured with this new sequence to an established method of global Y_v (Liu et al., 2016). Finally, tradeoff between in-plane and through-plane resolution in 3D acquisition was investigated.

Methods

Pulse sequence

As shown in Figure 4-1, the proposed sequence is a multi-gradient echo phase contrast sequence. Using the phase contrast principle, a complex difference (CD) image can be obtained by the complex subtraction of two images acquired with opposite gradient polarity (green gradients in Figure 4-1). Only the flowing blood signal is present in the CD image, thereby isolating pure blood signal in the presence of tissue partial voluming. The multi-gradient echo acquisition then allows the measurement of blood R_2^* (or T_2^*). Flow compensation was employed in both y and z directions for the first echo. Additional flow compensation in the y-direction was applied for all later echoes using schemes developed by Xu et al. (Xu et al., 2014). These strategies are important in minimizing mis-match in spatial coordinates of the measured signal, so-called oblique flow artifacts (Frank et al., 1992). Fly-back gradients are applied in the readout direction to ensure identical geometric distortion along x-direction across all echoes (Lu et al., 2008). Compared to a previous sequence which was based on a similar principle but used CPMG-T_2 preparation pulses (Krishnamurthy et al., 2014a), the present sequence is more time efficient in three ways. First, the multiple echoes are acquired in one TR, rather than in separate TRs. Second, the CPMG-T_2 sequence is associated with higher RF power deposition, thus a relatively long TR (e.g. 668 ms) is needed

to accommodate the SAR limits. Third, since T_2^* is considerably shorter than CPMG-T_2, a shorter echo time can be used for the same amount of signal attenuation, which reduces TR. These improvements add up to approximately 40 times reduction in scan time compared to the previous method (Krishnamurthy et al., 2014a), and allow the extension of the technique from 2D to 3D without drastically increasing the scan duration. To be consistent with the naming convention of the previous method (Krishnamurthy et al., 2014a), I refer to the present sequence as T_2-Relaxation-Under-Phase-Contrast 3D version (TRU-PC 3D).

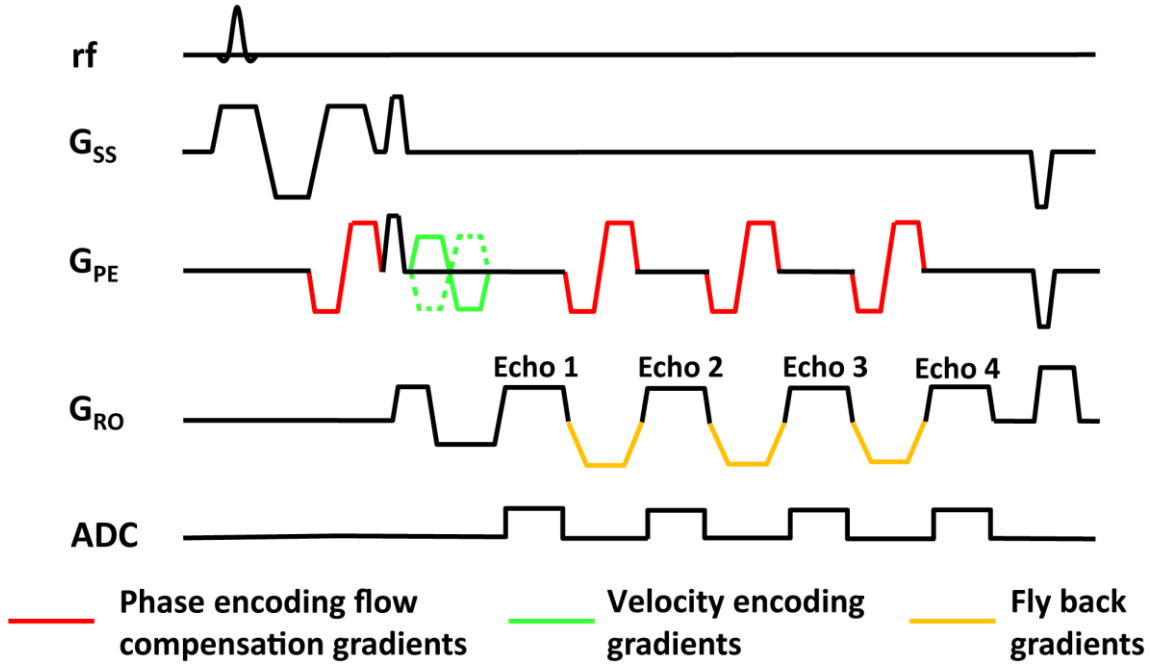

Figure 4-1: Sequence diagram of TRU-PC 3D. Key sequence components are displayed in color.

Theory

The blood signal as measured in the CD image is related to flow velocity and cutoff velocity of the sequence, V_{enc}, by:

$$\mathrm{CD} = 2M_{blood}\left|sin(\frac{\pi v}{2V_{enc}})\right| \quad [3\text{-}1]$$

where M_{blood} is the magnetization of the blood at given TE and v is the velocity of the blood along the encoding direction (typically anterior-posterior, foot-head, or left-right). M_{blood} is related to TE, TR, and flip angle of the sequence as well as its volume fraction in the voxel, and can be written as:

$$M_{blood}(TE) = M_0 \cdot f_{blood} \cdot \frac{\sin\alpha\cdot(1-e^{-TR\cdot R_{1,blood}})}{1-\cos\alpha\cdot e^{-TR\cdot R_{1,blood}}} \cdot e^{-TE\cdot R^*_{2,blood}} \quad [3\text{-}2]$$

where M_0 is the total equilibrium magnetization in the voxel, f_{blood} is the fraction of blood, and α is the flip angle. When I combine Eqs. [1] and [2], the CD signal at the given TE can be written as:

$$CD(TE) = 2M_0 \cdot f_{blood} \cdot \left|sin(\frac{\pi v}{2V_{enc}})\right| \cdot \frac{\sin\alpha\cdot(1-e^{-TR\cdot R_{1,blood}})}{1-\cos\alpha\cdot e^{-TR\cdot R_{1,blood}}} \cdot e^{-TE\cdot R^*_{2,blood}} \quad [3\text{-}3]$$

In this equation, if I combine the TE-independent terms into a S_0, the signal becomes:

$$CD(TE) = S_0 e^{-TE\cdot R^*_{2,blood}} \quad [3\text{-}4]$$

The $R^*_{2,blood}$ can then be estimated from a mono-exponential fitting of the multi-TE data.

In vivo experiment

The MRI experiment was carried out in a total of 13 young and healthy subjects (age, 27±7 years; range, 21-35, 3 males) using a 3 Tesla MRI scanner (Philips Healthcare, Best, The Netherlands). The protocol was approved by Institutional Review Board at Johns Hopkins University. All subjects gave informed written consent before participating in the study. The RF transmission used the body coil, and the receiving coil was a 32-channel head coil. Three sub-studies were conducted to characterize different aspects of the technique, which are described separately in the following sections.

Feasibility and reproducibility study

Four subjects participated in this sub-study. Each participant underwent two TRU-PC 3D scans and a time-of-flight (TOF) angiogram scan, which was used in data analysis (see below) to differentiate veins from arteries in the TRU-PC 3D image. The imaging parameters for TRU-PC 3D were as follows: 3D gradient echo readout, sagittal orientation, anterior-posterior phase encoding,

FOV=200×200×85 mm^3, acquisition matrix=288×284×17, voxel size=0.7×0.7×5 mm^3, bandwidth=217 Hz, V_{enc}=9 cm/s in anterior-posterior direction, flip angle/TE/ΔTE/TR= 15.6º/13 ms/14 ms/60 ms, 4 echoes were acquired for each TR. In choosing echo time parameters, our goal was to use the shortest possible TE and ΔTE for given gradient amplitude and slew rate while maintaining flow compensation. The number of echoes was determined based on considerations of sufficient signal decay while minimizing TR (thereby scan duration). The scan time of each TRU-PC 3D was 9.8 min. The imaging parameters for TOF MRI were as follows: 3D gradient echo readout, axial slice orientation divided into 10 chunks, FOV=170×170×150 mm^3, acquisition matrix=356×226×300, voxel size=0.48×0.75×1 mm^3, flip angle/TE/TR=20º/3.5 ms/25 ms, Sensitivity encoding (SENSE) factor=2, scan duration=10.2 min. Note that the FOVs of the TRU-PC 3D and TOF scans are not matched because they are acquired in different orientations. In post-processing, however, these images are resliced to match each other.

Hyperoxia study

A hyperoxia study was performed to test the sensitivity of TRU-PC 3D to expected venous oxygenation change when the subject inhales high oxygen

content gas. Four subjects participated in this sub-study. During the experiment, the subjects were instructed to inhale room air and high oxygen content gas sequentially (95% O_2 and 2.5% CO_2 balanced with N_2) through mouth piece as described previously (Lu et al., 2014). The gas type the subject inhaled was controlled though a three way valve. During the room air period, a TRU-PC 3D and global oxygenation sequence, TRUST MRI (Lu & Ge, 2008), were performed. The TRU-PC 3D protocol was identical to that used in the feasibility study described above. The TRUST sequence was described in previous literature (Lu & Ge, 2008) and had a duration of 1.2 minutes. A TOF angiogram scan was then started. Half way (approximately 5 minutes) into the TOF scan, the gas valve was switched to allow the participant to start breathing the hyperoxic gas. By the time the TOF scan is completed, the participant would have breathed the hyperoxic gas for about 5 minutes and is expected to have reached a new steady state. Then TRU-PC 3D and TRUST MRI were performed again under the hyperoxic state.

Resolution-dependence study

I studied the tradeoff between in-plane and through-plane resolution in a full-brain coverage scan. Two TRU-PC 3D protocols were compared in 5

subjects. The first protocol used a high in-plane resolution and a low through-plane resolution with a voxel size of 0.7×0.7×5 mm^3, a matrix of 288×284×31, and a scan duration of 17.9 min. The other protocol used a more isotropic voxel size of 1.5×1.5×2 mm^3, acquisition matrix of 133×132×77, and a scan time of 20.6 min. A TOF angiogram was also performed.

In vivo data analysis

The TRU-PC 3D images were reconstructed and corrected for eddy-current induced phase artifact as described in (Krishnamurthy et al., 2016). To focus our analysis on voxels containing measurable blood vessels, the complex difference images from all TEs were averaged and a threshold (10 times the standard deviation of the noise sampled from a non-vessel control region) was applied to obtain a preliminary vessel mask. Further analysis of blood oxygenation was only conducted on voxels within the mask.

Blood oxygenation was quantified on two spatial levels, region-of-interest (ROI) level and voxel-wise level. In the ROI analysis, nine ROIs were drawn on the vessel mask to encompass five mid-sagittal and four cortical veins: anterior and posterior superior sagittal sinus, internal cerebral veins, straight sinus, left transverse sinus, bilateral anterior and posterior cortical

veins. The complex difference signal inside the ROI was averaged for each TE and fitted monoexponentially for R_2^*. The R_2^* was further converted to oxygenation according the R_2^*-Y calibration plot, which is discussed in the next section.

For voxel-wise analysis, an isotropic Gaussian smoothing (6mm full-width-half-maximum, FWHM) was applied to the masked complex difference images. Voxel-wise fitting was performed on voxels within the vessel mask. To avoid arterial vessels and to remove voxels with low signal stability, the following four steps were performed to refine the mask used for final display. First, an artery mask was obtained by analyzing the time-of-flight angiogram using the Amira software (FEI Visualization Sciences Group, Hillsboro, Oregon) and voxels in the arterial mask were eliminated from the blood R_2^* map. Second, 95% confidence interval of the R_2^* estimation was evaluated and voxels that have a confidence interval of greater than the estimated R_2^* value were discarded. Third, the S_0 value from the R_2^* fitting, which denotes the intensity of blood signal without any R_2^* weighting, was evaluated and voxels with an S_0 of less than a threshold (1×10^5 A.U. for voxel size $0.7\times0.7\times5$ mm^3 and 3×10^5 A.U. for voxel size $1.5\times1.5\times2$ mm^3) were discarded. Note that I used a group-level threshold for S_0. An alternative approach would be to use an

individual threshold based on each data's SNR. I did not use an SNR-based threshold because the estimation of noise in S_0 is not trivial as it is a fitted parameter rather than experimental measure. Finally, small clusters with a volume of less than 135 mm^3 were removed. The final R_2^* map was converted to oxygenation map using the calibration plot. For 3D display purposes, I employed the Amira software to convert the oxygenation map to a 3D model. The oxygenation value was then displayed on Paraview (Ayachit, 2015) in vtk format.

In vitro blood experiment and analysis

To allow the conversion of blood R_2^* value to oxygen saturation fraction, I conducted a set of calibration experiments using bovine blood, which has physiological and MR properties comparable to human blood (Benga & Borza, 1995). Note that the calibration experiment does not need to be done for every subject or every study. Once a calibration plot is established, it can be used for all future scans using an equivalent pulse sequence. Fresh Bovine blood was obtained from a local slaughtering house in the morning of each experimental day. Sodium citrate was added to the blood for 25 mM concentration to avoid coagulation. The experiments were completed within 8 h after collection to

minimize the effect of degradation. Adjustment of hematocrit (Hct) level was achieved by centrifuging the blood and adding or removing plasma. Four Hct levels (36%, 39%, 45% and 53%) were studied in 3 batches of blood. Adjustment of blood oxygenation was achieved by exposure to room air (to increase oxygenation) or nitrogen gas (to decrease oxygenation). For blood MR measurements, 10 ml of blood was placed in a 27 mm-diameter plastic tube and kept at 37 ^{o}C with water bath to match the physiological condition. The blood oxygenation and hematocrit levels were measured by a blood gas analyzer (ABL830m, Radiometer America Inc., Westlake, OH) immediately before and after the MR session and their averaged value was used in the analysis. The imaging protocol was the same as the in vivo protocol used in the reproducibility study, except that the FOV was reduced to 90×90 mm^2 to shorten the scan time to 4.4 min. The MR session for one oxygenation and Hct level was completed within 6 min. According to our previous experience (Krishnamurthy et al., 2014b; Lu et al., 2012), blood cell precipitation is minimal within this short time.

For data analysis, ROIs were drawn in the center of three consecutive slices encompassing the blood sample. The signals in the ROIs were averaged and fitted to a mono-exponential equation:

$$S = S_0 e^{-TE \cdot R_2^*}$$

The resulting R_2^* values were then fitted to a quadratic function of blood oxygenation, Y (Silvennoinen et al., 2003; Zhao et al., 2007):

$$R_2^* = A^* + C^*(1 - Y)^2$$

This fitting was performed for each Hct level. Linear interpolation of the R_2^*-Y curves across Hct then yields a 3D calibration plane for all physiological Hct levels.

The calibration plot was used to convert in vivo R_2^* values to oxygenation. In this study, I assumed an Hct of 0.42 for male and 0.40 for female. Because human scans tend to have more macroscopic inhomogeneities due to imperfect shimming, this will increase R_2^*. Thus, a fixed correction factor $R_{2,corr}^*$ was subtracted from in vivo R_2^* before the conversion. In this study, $R_{2,corr}^*$ was assumed to be 8.8 s^{-1} based on the literature (Wansapura et al., 1999). Note that since a fixed $R_{2,corr}^*$ is used, this assumption will not change any inter-subject or inter-regional differences of the oxygenation results.

Results

Blood R_2^* and its dependence on oxygenation and Hct

The fitting of in vitro blood signal as a function of TE was reliable, and R_2^* could be estimated from all blood samples. Figure 4-2a shows the dependence of blood R_2^* on oxygenation for a range of Hct values. As expected, blood R_2^* is strongly dependent on Y. For a typical Hct level of 39%, R_2^* of a venous blood sample with oxygenation of 60% was 28.9 s^{-1}, while R_2^* of a fully oxygenated blood sample was 12.7 s^{-1}. In contrast, blood R_2^* is less affected by Hct. Fitting the R_2^* value to a quadratic equation of Y yielded coefficients A and C, which are listed in Table 4-1 for each Hct value. The Hct-specific 2D curves were extended to a 3D surface plot, by interpolating the curves along the Hct dimension, so that one can obtain an R_2^*-Y plot for any Hct value within the physiological range (Figure 4-2b).

Hct level	A (s^{-1})	C (s^{-1})
36%	12.6	83.5
39%	12.7	101.1
45%	13.4	101.2
53%	15.2	148.5

Table 4-1: The fitted coefficients A and C for different Hct levels.

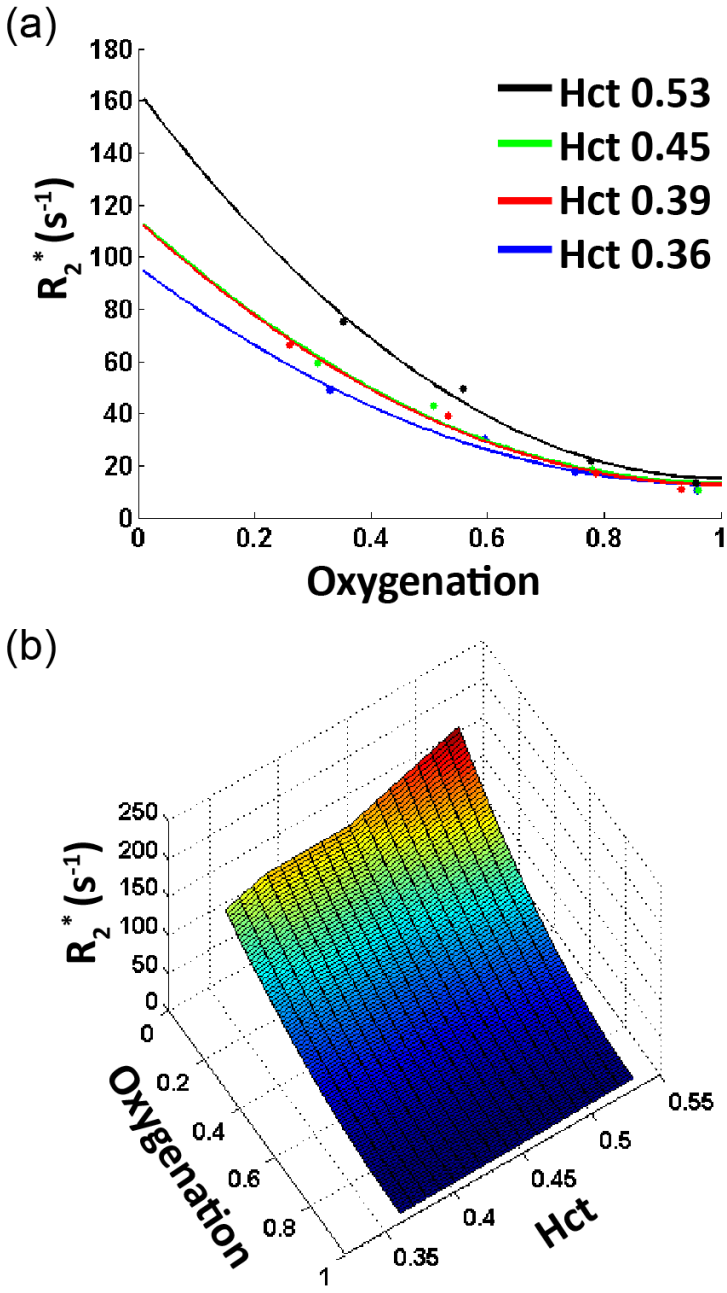

Figure 4-2: Summary of in vitro blood experiments. (a) R_2^* as a function of blood oxygen (Y) at several Hct levels. (b) Three-dimensional relationship among R_2^*, Y, and Hct.

Feasibility study of TRU-PC 3D

An example of complex difference images from a TRU-PC 3D scan are shown in Figure 4-3a. Multiple slices along the left-right direction have been combined (via maximum intensity projection) for display purposes. Large venous vessels such as internal cerebral veins (arrows) and superior sagittal sinus (arrows heads) are discernible in the images. Furthermore, small cortical and sub-cortical vessels that do not have designated names are also visible, which is an advantage of the 3D method in comparison with previous single-slice technique. As echo time increases (Figure 4-3b), the signal intensity decreases, the rate of which is blood R_2^*.

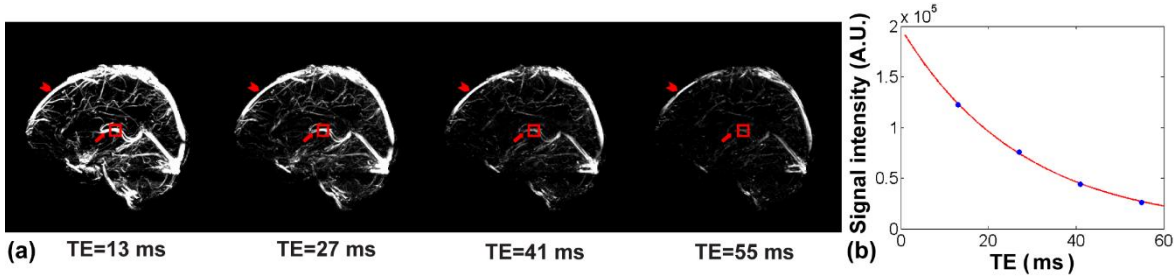

Figure 4-3: Representative TRU-PC 3D data in volunteer. (a) Complex difference images from TRU-PC 3D as a function of TE. The complex difference image of the sequence is expected to contain signals from vessel only. Images have been maximum-intensity projected for display purpose. Arrow head indicates superior sagittal sinus. Arrow indicates internal cerebral

veins. Red box indicates ROI from which the data of Panel b is derived. (b) Complex difference MR signal as a function of TE. The solid curve indicates the fitting results.

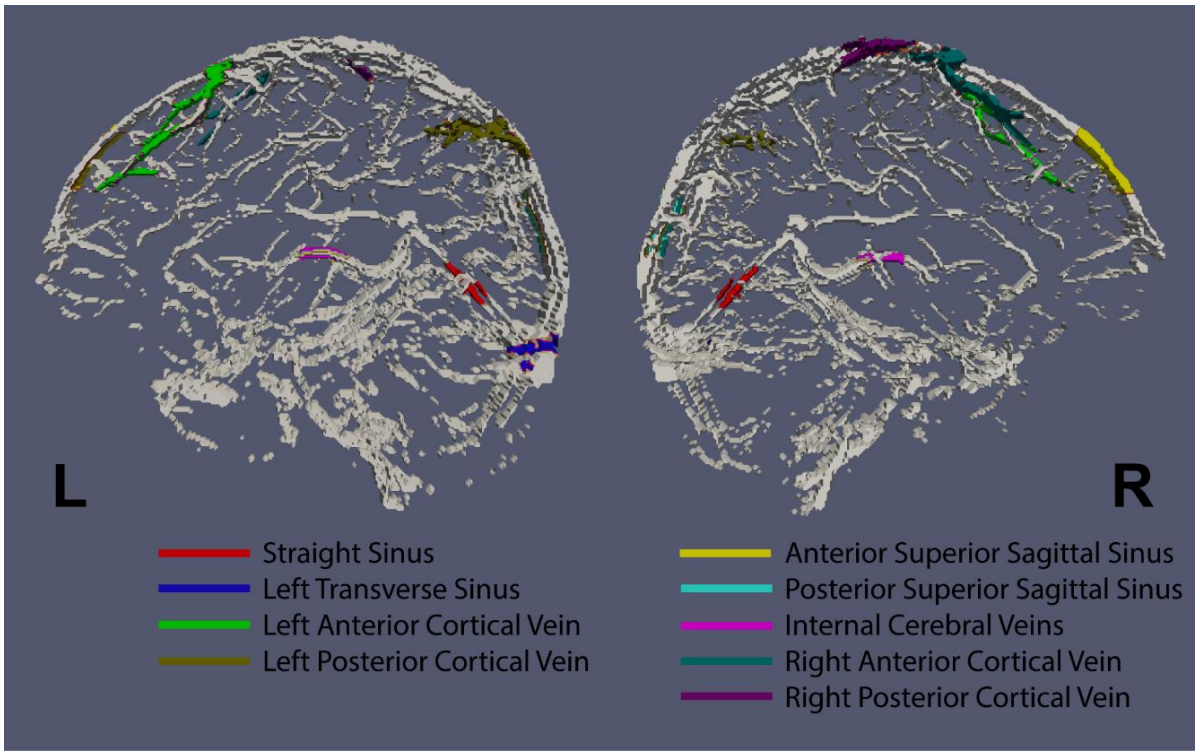

Figure 4-4: Regions of interest (in color) overlaid on complex difference image. The ROIs were drawn manually and the signals within each ROI were averaged and fitted. The resulting oxygenation values are listed in Table 4-2.

ROI results of 9 different venous structures (Figure 4-4), of which five were major veins and four were cortical veins, are listed in Table 4-2. The venous oxygenation ranged from 57% to 72%, which is in agreement with reported Y_v values in the literature (Gibbs et al., 1942; Ibaraki et al., 2008; Lu et

al., 2011). Results of intra-session test-retest reproducibility are also shown in Table 4-2. The average coefficient-of-variation (CoV) across runs is 3.0%.

ROI Location	Y_v	CoV
Anterior Superior Sagittal Sinus	71.3%±4.9%	2.9%
Posterior Superior Sagittal Sinus	64.8%±11.0%	5.4%
Internal Cerebral Veins	69.3%±8.9%	2.4%
Straight Sinus	72.0%±9.3%	3.5%
Left Transverse Sinus	57.0%±7.9%	2.6%
Right Anterior Cortical Vein	70.25%±3.0%	1.8%
Right Posterior Cortical Vein	68.3%±4.3%	2.3%
Left Anterior Cortical Vein	70.3%±2.2%	3.1%
Left Posterior Cortical Vein	67.8%±7.8%	3.3%

Table 4-2: Average oxygenations and CoVs for 9 venous ROIs in Figure 4-4.

3D oxygenation maps of veins and arteries (separated based on TOF angiogram) as well as their combination are displayed in Figure 4-5a. It can be seen that, in the venous oxygenation map, most of the voxels have blue color, consistent with the expected lower oxygenation range. In contrast, the arterial oxygenation map largely shows red color, indicative of higher oxygenation

values. Histograms of all voxels of all subjects (N=13, 3M, Age 26.5±3.6 years old) are displayed in Figure 4-5b, providing a quantitative summary of the oxygenation values in the voxels.

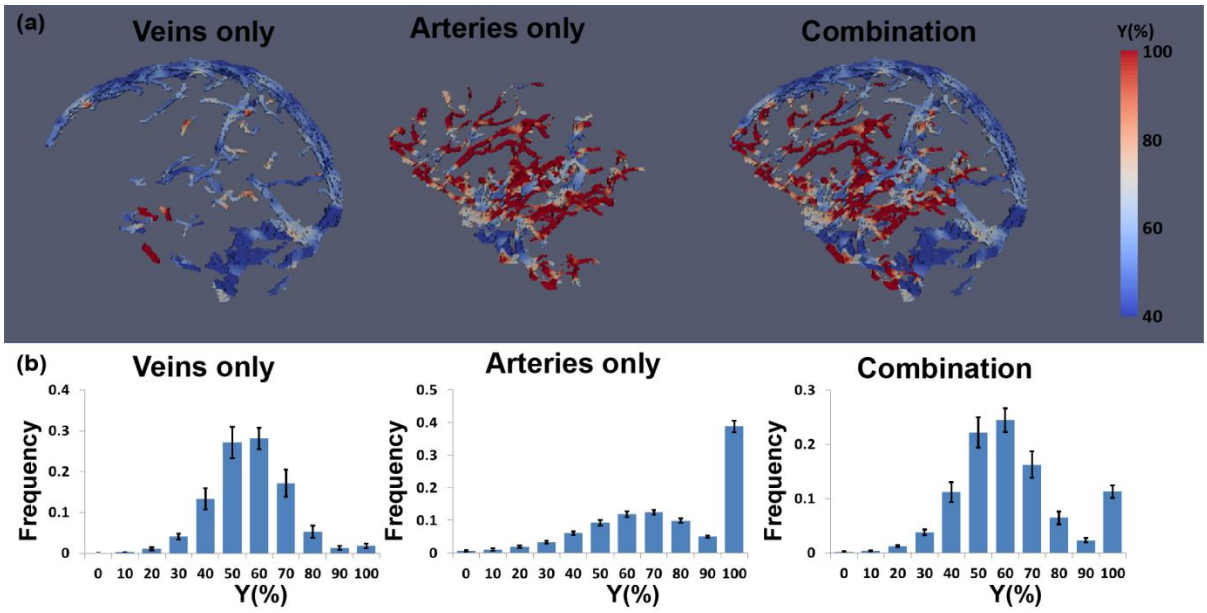

Figure 4-5: Quantitative oxygenation maps obtained from TRU-PC 3D. (a) An example of 3D oxygenation maps of veins only, arteries only, and their combination. (b) Histogram of oxygenation values in each map. The results of all participants were averaged, with error bars indicating standard errors across individuals.

Hyperoxia study

Hyperoxia increased the subjects' end-tidal O_2 from 13.3%±0.3% to 85.0%±2.9%, while end-tidal CO_2 did not show a change (5.8%±0.1% and

5.6%±0.3% during room-air and hyperoxia, respectively). Venous oxygenation maps during room-air and hyperoxia are shown in Figure 4-6a. It can be seen that blood oxygenation clearly becomes higher during hyperoxia, consistent with the known effects of this physiological manipulation (Xu et al., 2012). ROI results are shown in Figure 4-6b, which revealed that venous oxygenation increased significantly ($P<0.05$) in every region and by 10.8% on average.

Venous oxygenation values measured by TRU-PC 3D were compared with those measured by a well-established global method, TRUST MRI. For this analysis, data from 8 subjects were used, including 4 participants from the hyperoxia study (who provided 4 hyperoxia data points and 4 room-air data points) and 4 participants from the feasibility study (who provided 4 room-air data points). The average oxygenation from TRU-PC 3D was 65.0%±7.4%, which was similar ($P=0.8$) to the TRUST results of 64.8%±7.7%. Figure 4-7a showed a scatter plot of individual participants, revealing a strong correlation ($P<0.001$) between the two methods. The measurement from two techniques are also plotted in Bland-Altman plot in Figure 4-7b. The mean difference between two measurement is -0.77%, which shows no significant difference than 0 according to one-sample t-test ($P=0.43$), suggesting little bias between two measurements. All the difference data points fall within 95% limits of

agreement (average difference ± 1.96 standard deviation of the difference), demonstrating good agreement between two measurements.

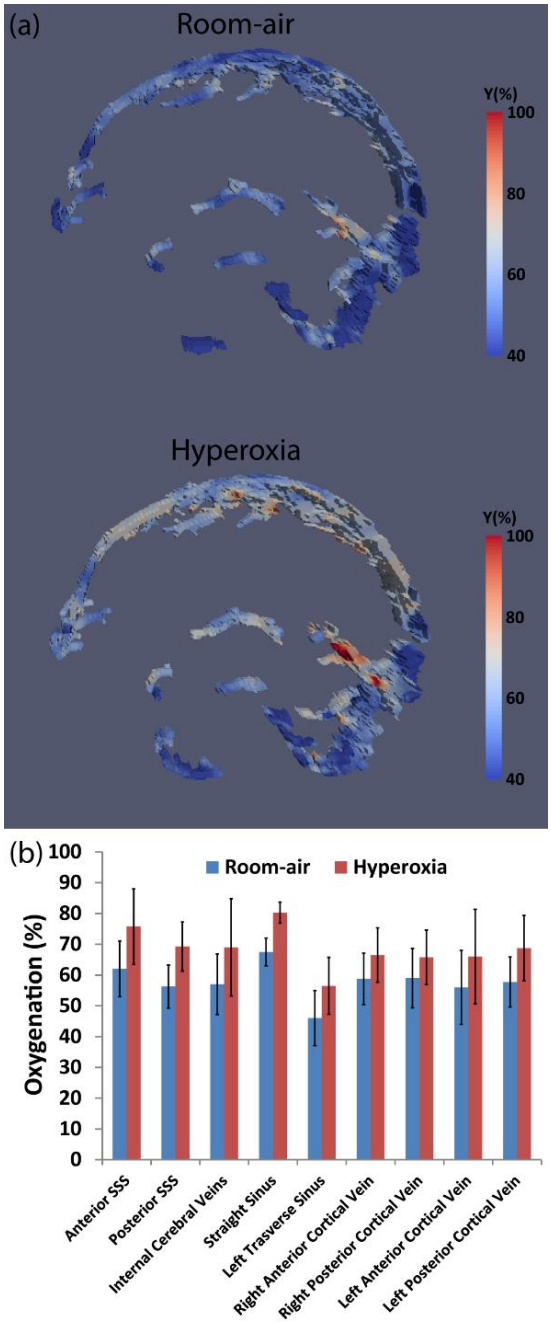

Figure 4-6: Summary of TRU-PC 3D results during hyperoxia challenge. (a) Representative venous oxygenation maps under normoxia and hyperoxia. (b) Region of interest results for nine ROIs. Error bars indicate standard errors. SSS: Superior sagittal sinus.

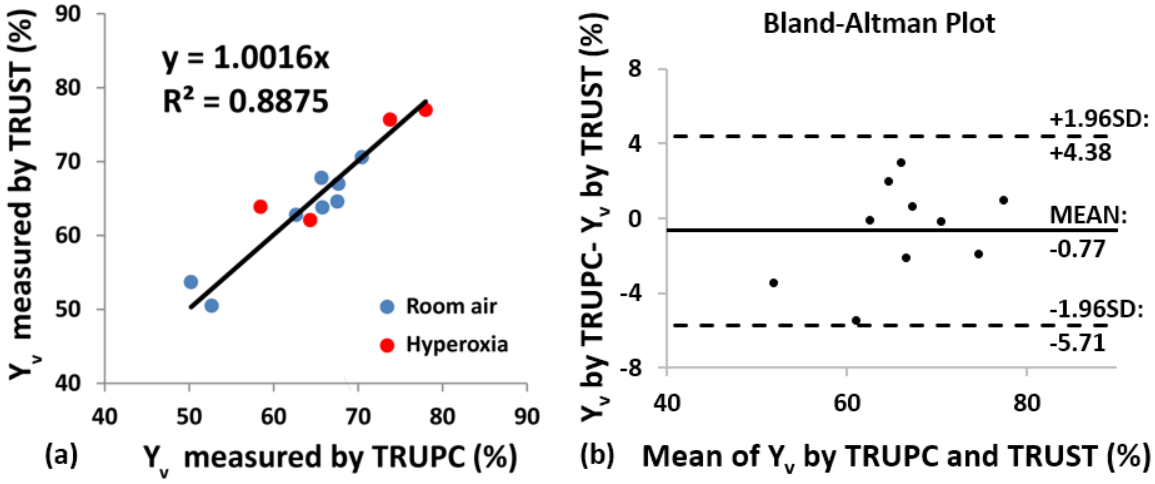

Figure 4-7: (a) Scatter plot between oxygenation values measured with TRU-PC 3D and those from TRUST MRI. Blue dots represent results under room-air breathing. Red dots represent results under hyperoxia. Four subjects participated in both room-air and hyperoxia experiments. Four additional subjects participated in room-air only. (b) Bland-Altman plot of the oxygenation measurement between TRU-PC 3D and TRUST.

Resolution-dependence study

Figure 4-8 shows venous oxygenation maps acquired at two spatial resolutions (see https://youtu.be/ikpw9WgCkig for movie). Figure 4-8a was

acquired with a high in-place resolution (0.5×0.5 mm^2), but a coarse through-plane resolution (5 mm). Figure 4-8b was acquired with a more isotropic voxel dimensions of 1.5×1.5×2 mm^3. It can be seen that each scheme has advantages and disadvantages. The scan with high in-plane resolution shows good spatial acuity when viewed sagittally, but appears poor in the coronal view. A movie for the two maps is provided in the supporting information for better view. The isotropic scan shows a more consistent image when viewed from different directions. ROI analysis showed no difference (P>0.05 for all ROIs) in oxygenation between the two methods, with 56.0%±9.0% (N=5) for the non-isotropic protocol and 57.9%±9.3% for the isotropic protocol.

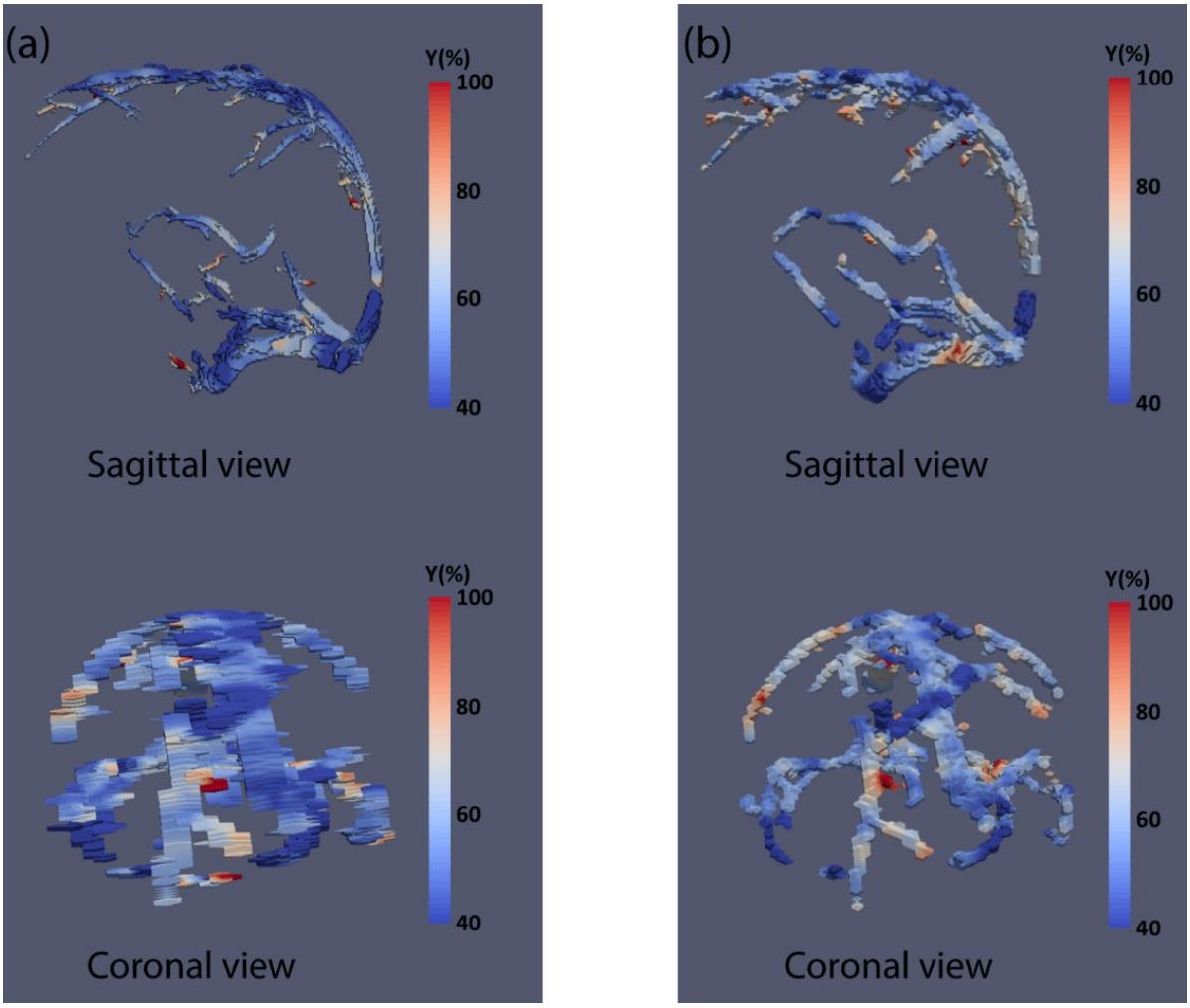

Figure 4-8: Y_v maps from one representative subject using two spatial resolutions. (a) voxel size 0.7×0.7×5 mm^3; (b) voxel size 1.5×1.5×2 mm^3. Top panels show sagittal view and bottom panels show coronal view.

Discussion

This study presented a technique for quantitative assessment of brain venous oxygenation without using exogenous contrast agent. The technique is based on a novel pulse sequence and, compared to previous methods, has

extended spatial coverage. The performance of this new method was demonstrated in a group of healthy volunteers and the results showed oxygenation values within the typical physiological range. The method was found to be reproducible with intra-session CoV of 3% and was sensitive to oxygenation changes induced by hyperoxia. The method showed good agreement with a validated technique TRUST MRI. In vitro experiments were also performed to characterize the relationship between blood R_2^* and oxygenation, which was used to convert in vivo R_2^* results to oxygen saturation fractions.

Physiological considerations

The brain represents approximately 2% of the body weight, but consumes about 20% of the energy (Albers & Siegel, 1999). Thus, the rate of oxygen metabolism is an important marker for brain development, aging, and diseases. Venous oxygenation is closely related to cerebral metabolic rate of oxygen ($CMRO_2$) and oxygen extraction fraction (OEF), $OEF = \frac{(Y_a - Y_v)}{Y_a}$ and $CMRO_2 = CBF \cdot (Y_a - Y_v)$. Among these physiological parameters, arterial oxygenation (Y_a) is relatively easy to measure and cerebral blood flow (CBF) can also be evaluated with a number of non-invasive techniques. Assessment of Y_v has

been a bottle neck in terms of measurement technologies. ^{15}O PET is the current gold standard, but it is rarely used due to complexity in procedures. Therefore, at present, there is not an established method to measure brain venous oxygenation in routine clinical practice.

Recently, there has been a growing interest to develop new MR methods to measure Y_v. Indeed, global Y_v measurements using MRI have been successfully applied to Alzheimer's disease (Thomas et al., 2016), multiple sclerosis (Ge et al., 2012), genetic disease of brain metabolism (Pascual et al., 2014b), sickle cell (Bush et al., 2014), anorexia (Sheng et al., 2015), end-stage renal disease (Zheng et al., 2016), congenital heart disease (Jain et al., 2014) and cocaine addiction (Liu et al., 2014). In addition, it has been used in studies of brain development and aging (Lu et al., 2011). However, application of such techniques in focal brain diseases such as brain tumor and stroke requires regional Y_v methods. The present work represents one of such effort.

Technical considerations

MRI techniques for regional Y_v quantification can be divided into 4 categories. The first one is a qBOLD method based on biophysical modeling of blood oxygenation on tissue transverse relaxation rate (He & Yablonskiy,

2007). The second one is based on calibrated fMRI. In this method, two gas challenges, for example hyperoxia and hypercapnia, are applied to induce alteration in CBF and BOLD MRI signal. By using a mathematical model to solve the interplay among these physiological parameters, CBF, OEF, and $CMRO_2$ can be simultaneously estimated (Gauthier & Hoge, 2012; Wise et al., 2013). The third category is based on the effect of paramagnetic deoxyhemoglobin on MR signal phase (Fan et al., 2014; Fernandez-Seara et al., 2006; Xu et al., 2014). The method proposed in the present work represents a fourth category, which is based on the relationship between oxygenation and R_2/R_2^* of the blood. The methods in this category involve advanced pulse sequences that are capable of isolating venous blood signal from surrounding tissue, thereby minimizing partial voluming effects. Several techniques have been proposed including those based on spin labeling principles such as TRUST (Lu & Ge, 2008), QUIXOTIC (Bolar et al., 2011) and VSEAN (Guo & Wong, 2012), and those based on flow-encoded phase contrast such as TRU-PC (Krishnamurthy et al., 2014a). However, to date, such methods are spatially limited to a single slice acquisition.

The present work represents the first demonstration of 3D venous oxygenation using blood transverse relaxation measurements. Compared to the

2D TRU-PC method reported by Krishnamurthy et al. (Krishnamurthy et al., 2014a), the present 3D technique uses a R_2^* approach rather than R_2. This change was made primarily based on scan time considerations. The previous 2D method required approximately 7 minutes to acquire one slice, thus it was not feasible to extend it to 3D acquisitions. One of the reasons for the long scan time of 2D TRU-PC was that the 180° pulses in the R_2 preparation module of the sequence result in considerable RF power deposition and, consequently, a long TR (>668 ms) must be used to be compatible with SAR limits. The 3D sequence proposed in this study does not use refocusing RF pulses, and thus a short TR of 60 ms can be used, which can shorten the scan duration by 11 times with this factor alone. A second factor that reduced scan duration in the TRU-PC 3D technique was that multiple echoes were acquired in the same TR, unlike the 2D method in which different TRs must be used for different T_2-preparation durations. This factor could shorten the scan time by another 4 fold. The scheme of acquiring all echoes in one TR also minimized the effects of subject motion or physiological fluctuations. Collectively, these improvements allowed the assessment of 3D venous oxygenation with only a modest increase in scan time.

The present study used a V_{enc} of 9 cm/s for flow encoding of cerebral veins. This value is approximately the mid-point of the large vessel (15 cm/s) and small vessel (4 cm/s) V_{enc} values used in our previous study (Krishnamurthy et al., 2016). Previous literature has suggested the following velocity range for various venous vessels in the brain: superior sagittal sinus 15.2 cm/s (Gideon et al., 1996), straight sinus 10.4 cm/s (Stolz et al., 1999), the great vein 9.8 cm/s (Stolz et al., 1999), internal cerebral veins 6.1 cm/s (Stolz et al., 1999), and cortical vein 7.1 cm/s (Yamada et al., 1997). Thus, the V_{enc} I chose provides a good balance of sensitivity between large and small veins. If more scan time is available, it is recommended to utilize more than one V_{enc} value so that a better sensitivity could be obtained for a range of vessels.

The method proposed in the present work employed flow encoding in the anterior-posterior direction, but can be expanded to the three-directional space. Such expansion could adopt schemes used previously in 3D phase-contrast MRI (Haacke et al., 1999) such as Hadamard encoding. In this encoding scheme, four types of flow-encoding gradients would be used in the experiment and various combinations of these four complex images will yield flow-encoded signal in each of the x, y, and z directions. The three flow-encoded signals can then be combined geometrically to yield the final signal intensity for R_2^* fitting.

The present work has primarily focused on the measurement of oxygenation in cerebral veins. It is also possible to measure oxygenation in arteries (e.g. Figure 4-5). However, it should be pointed out that, due to the quadratic nature of the blood relaxometry curve (e.g. Figure 4-2), the sensitivity of our technique is expected to be lower in arterial oxygenation range. Additionally, since arterial blood is originated from the heart and its oxygenation is the same across the body, this value can be measured more conveniently in the periphery using pulse oximetry.

Limitations

While the switch from R_2 to R_2^* measurement increased acquisition efficiency and reduced scan time, it also increased the susceptibility of the sequence to several other factors. In my oxygenation map, I observed some high oxygenation values in the venous map and some low oxygenation values in the arterial map (Figure 4-5). One possible reason is that, at the time of the flow-encoding (i.e. time of the bipolar gradient), the blood spins that are later measured in the different echoes are physically in different locations. That is, different echoes measured different spins. These spins may have slightly different flow velocity, thus may bias the R_2^* estimation. Another possible

reason for the low oxygenation values in the arterial voxels at the base of the brain could be that the blood signals being measured in the later echoes did not experience the excitation RF pulse.

Another limitation is that R_2^* is more sensitive to shimming condition and macroscopic inhomogeneity, compared to R_2. Because in vitro blood samples are more homogeneous and easier to shim relative to in vivo imaging, this results in some discrepancy between in vitro blood calibration data and in vivo blood R_2^* (Zhao et al., 2007). I therefore added a correction factor based on literature values of macroscopic R_2', before conducting the calibration of blood R_2^*. The resulting oxygenation showed good correspondence with the R_2 based TRUST results, suggesting that our assumed macroscopic R_2' is generally valid. However, since shimming condition could vary across brain regions, it would be ideal to conduct macroscopic inhomogeneity correction on a voxel-by-voxel basis (He & Yablonskiy, 2007; Yablonskiy et al., 2013). Since our TRU-PC 3D sequence produced multi-echo data with phase information, I calculated phase maps and further estimated field gradient maps using phase values of adjacent voxels. While these maps provided B_0 inhomogeneity information in the majority of the brain, in regions near and inside veins such computation failed unfortunately. This is because venous voxels have additional susceptibility

effects from deoxyhemoglobin, which renders the B_0 inhomogeneity estimation inaccurate. Thus, in order to estimate B_0 inhomogeneity in venous voxels, a higher resolution phase mapping scan, in which each TRU-PC 3D voxel is divided into several sub-voxels, is needed. However, given that our TRU-PC voxel size is already on the order of 1 mm, further dividing it into smaller voxels would be difficult from the standpoint of scan time and image SNR. High resolution used in our TRU-PC 3D sequence does, however, help limit the extent of B_0 inhomogeneity in our data. Furthermore, since I used phase-contrast scheme to isolate sub-voxel venous signal, it is likely that the B_0 inhomogeneity of our venous signal is smaller than that of the entire voxel.

Finally, conversion of blood R_2^* to oxygenation requires the knowledge of hematocrit. Hematocrit would vary across individuals and may alter under certain pathological conditions such as anorexia (Sheng et al., 2015) or Sickle cell anemia (Jordan et al., 2016). Therefore, for accurate estimation of blood oxygenation, it is desirable to measure hematocrit on each individual using either blood sampling or MRI methods (Qin et al., 2011; Varela et al., 2011; Wu et al., 2010). Furthermore, it is known that microvessels have lower hematocrit values compared to macrovessels (Oldendorf et al., 1965; Sarelius & Duling, 1982). Because the diameters of the vessels relevant for our study (>1

mm) are much larger than the diameter of a red blood cell (8 μm), I assume that the hematocrit does not change across the vessels that are visible with TRU-PC 3D.

Conclusion

I have developed a quantitative technique to map venous oxygenation in 3D based on blood R_2^* relaxometry. The oxygenation values obtained were consistent with previous reports and also compatible with a validated global method performed on the same participants. Intra-session test-retest assessment revealed good reproducibility of the method. Sensitivity of the method to detect oxygenation alterations due to hyperoxia was demonstrated. This technique may have the potential to monitor oxygenation abnormalities in focal brain diseases.

CHAPTER FIVE

Other ways to measure the neural activity

During the course of my research, I have also participated in studies to assess the neural activity using methods different than cerebral venous oxygenation techniques. These studies can be categorized by the methods they used into two groups: functional connectivity MRI (fcMRI) studies and electroencephalogram (EEG) studies. I will describe them one by one in details in the following part.

Resting-state functional connectivity MRI is a method using BOLD imaging to evaluate brain activity while the subjects are in resting state without performing any tasks. More specifically, the brain activity measured by fcMRI is the interactions between different brain regions through the synchronization of low frequency fluctuating BOLD signal (Biswal, 2012). fcMRI have been widely used to study neuroscience as well as the neurological diseases. In one study I have participated (Tung et al., 2013), fcMRI was employed to study the impact of a recent motor task to functional connectivity. Volunteers were instructed to perform a button press task inside the scanner. Their brains' functional connectivity was assessed before and after the motor task at resting

state. It was found that the connectivity between left and right motor cortices was significantly increased (P=0.002, N=24) as well as the amplitude of fluctuations in such regions after the motor task. These effects can last 5 min for connectivity and 15 min for amplitude of fluctuations. These findings suggest the existence of the physiological ripple effect from previous task to functional connectivity and therefore, fcMRI should be performed before any task fMRI or after a sufficient gap to such experiment.

I have also calculated the fractional amplitude of low-frequency fluctuations (fALFF), an index of resting state brain activity, to study its correlation with brain gene expression (Wang et al., 2015). fALFF is a region-specific index derived from fcMRI experiment as in the ratio between the power of low frequency signal and the power of whole signal. Several genes were identified as their regional expression levels were correlated with the fALFF in the default mode network regions and those genes were found to be associated with autism.

For the clinical application of fcMRI, I have looked at the change of functional connectivity in one tinnitus patient before and after treatment of an antioxidant drug, named carnitine (Gopal et al., 2015). I have found that functional connectivity was increased between the right and left auditory cortex

as the patient's hearing was improved after treatment, which may indicate the value of carnitine as a tinnitus treatment. Later in a group study of tinnitus patients (Gopal et al., 2017), I have also shown that the connectivity between right and left auditory cortices showed a trend of reduction (P=0.06) in tinnitus patients group comparing to the control group.

Electroencephalogram (EEG) is also one commonly used measurement of brain neural activity. EEG monitors the brain's electrophysiology by placing electrodes on the scalp and recording its electrical activity. The electrical activity it records is from the local current in the neurons of the brain.

GLUT-1 deficiency is a genetic disorder, in which the glucose transporter has lost part of its function, causing lack of the glucose accumulation in the brain. Thus, the patients suffer from brain-related symptoms such as medication-refractory infantile-onset seizures (Pascual et al., 2008). In the study of such patients (Pascual et al., 2014a), their spike-wave seizures events were captured by EGG before and after triheptanoin oil consumption. The triheptanoin oil is a medium-chain triglyceride, which was tested in the study for the hypothesis that it can fill the roles of glucose for GLUT1 deficiency patients. A significant decrease in seizure rate ($P<0.05$) was observed in all patients after triheptanoin oil consumption.

EEG was also applied to study the effect of hyperoxia to the neuron activity in the brain (Sheng et al., 2017). The previous findings have shown that the hyperoxia challenge will cause a reduced $CMRO_2$ (Xu et al., 2012). But the direct evidence from the neuron activity point of view is still lacking. The present study compared the EEG signal during the room air state and hyperoxia state. The significant reduction ($P<0.01$) was found at the power of α band (8-13 Hz) and β band (14-35 Hz) in the resting state EEG. Additionally, main peaks of visual ERP (visual-stimulation event-related potential) are delayed during hyperoxia compared to room air state ($P=0.04$ for N1 peak and $P=0.02$ for P2 peak). These findings indicated hyperoxia suppressed neural activity in the brain.

To conclude, besides venous oxygenation measurements, I also have applied fcMRI and EEG techniques to study normal brain physiology and neurological diseases. fcMRI and EEG each reflects different aspects of the neural activity than the venous oxygenation measurements. These three methods could be complimentary to each other in the future studies.

.

CHAPTER SIX

Conclusions and future directions

Conclusions

In the first part, I have applied a noninvasive 2D MRI technique, TRUPC to assess the effect of hypertension to regional venous oxygenation in the brain. The lower venous oxygenation in the frontal lobe and deep brain are associated with high systolic pressure. In addition, the volume reduction in hippocampus and thalamus is correlated with the decreased venous oxygenation in these regions. Imaging marker Y_v reported here may prove valuable in understanding of hypoxia, CBF and cortical volume reduction in these regions caused by the hypertension. However, the scope of the study has been limited by the 2D FOV in TRUPC. Therefore, in the second part, I have developed a quantitative technique to map venous oxygenation in 3D based on blood relaxometry. The oxygenation values obtained were consistent with previous reports and also compatible with a validated global method performed on the same participants. Intra-session test-retest assessment revealed good reproducibility of the method.

Sensitivity of the method to detect oxygenation alterations due to hyperoxia was demonstrated. This technique may have the potential to monitor oxygenation abnormalities in focal brain diseases. In the last part, I have also used functional connectivity MRI and electroencephalogram to investigate the neural activity in both pathological conditions and normal physiology of the brain

Future directions

Improvement of the techniques

There are several aspects to improve the TRUPC 3D technique. First, the acquisition time is a major concern for the technique. Currently, it will take 20 mins for a single whole brain scan, which could prevent it from wide clinical applications. This is due to the high resolution and the plain multi-gradient-echo acquisition scheme it used. The compress sensing has been combined with phase contrast previously at an acceleration factor of 3 (Basha et al., 2015), which could potentially speed up the TRUPC 3D as well. Second, the accuracy of the technique can be further improved. The blood spin has been flow compensated during the multi echo acquisition, thus can be encoded correctly to the actual position on the image at each echo. However, the velocity encoding happens before the acquisition, the velocity change during the echo has not

been compensated and therefore cannot be reflected in the velocity encoding right after the excitation. The unsynchronized encoding and acquisition could bias the signal, especially when the flow has sharp velocity or direction change. To address this issue, a tri-polar gradient can be added between echoes to compensate the linear acceleration. Third, smaller veins have low signal intensity, moving into higher field could boost the signal for the smaller veins. The biggest concern in R_2 mapping in high field, such as 7T is B_1 inhomogeneity, since B_1 field is directly related to the accuracy of the T_2 preparation pulses. This issue becomes less of a problem when mapping R_2^* using multi-gradient-echo with macroscopic field correction (Yablonskiy et al., 2013). Moreover, the R_2^* of blood is higher in higher field, which will require less total echo time to wait for sufficient decay of venous blood signal, as needed by R_2^* fitting. This can reduce the scan time and the flow effect due to multi-echo acquisition.

Measurement of $CMRO_2$

Cerebral metabolism rate of oxygen is another important biomarker of the oxygen metabolism in the brain, which is the combination of the information from venous oxygenation and cerebral blood flow. The $CMRO_2$ is

a direct reflection of neuron energy metabolism. The CBF information is not hard to obtain. It can be either from the perfusion measurement by arterial spin labeling MRI or from flux in each vein obtained by phase contrast MRI. However, the $CMRO_2$ mapping can be difficult due to the venous drainage territory is hard to be precisely determined when using the large vessel Y_v measurement. Therefore, the mapping of $CMRO_2$ has not been attempted in this dissertation. The mapping of venous drainage territory has been attempted by using spin labeling on the venous side (Wong & Guo, 2013) but with very limited results. This issue could be partially dealt by measuring the venous oxygenation in smaller veins. The smaller the vein, the less complicated the drainage territory of the vein can be. Compared to the large cortical vein TRUPC 3D can measure, the drainage of the smaller veins (~1mm diameter in size) is more defined. The pursuit of the small vein oxygenation measurement is highly desired in this case.

BIBLIOGRAPHY

Albers, R., & Siegel, G. (1999). Basic Neurochemistry: Molecular, cellular and medical aspects: Philadelphia, PA: Lippincott Williams & Wilkins.

Aliev, G., Smith, M. A., Obrenovich, M. E., de la Torre, J. C., & Perry, G. (2003). Role of vascular hypoperfusion-induced oxidative stress and mitochondria failure in the pathogenesis of Azheimer disease. *Neurotox Res, 5*(7), 491-504.

Alosco, M. L., Gunstad, J., Jerskey, B. A., Xu, X., Clark, U. S., Hassenstab, J., Cote, D. M., Walsh, E. G., Labbe, D. R., Hoge, R., Cohen, R. A., & Sweet, L. H. (2013). The adverse effects of reduced cerebral perfusion on cognition and brain structure in older adults with cardiovascular disease. *Brain Behav, 3*(6), 626-636.

Alosco, M. L., Gunstad, J., Xu, X., Clark, U. S., Labbe, D. R., Riskin-Jones, H. H., Terrero, G., Schwarz, N. F., Walsh, E. G., Poppas, A., Cohen, R. A., & Sweet, L. H. (2014). The impact of hypertension on cerebral perfusion and cortical thickness in older adults. *Journal of the American Society of Hypertension, 8*(8), 561-570.

Attwell, D., & Laughlin, S. B. (2001). An energy budget for signaling in the grey matter of the brain. *J Cereb Blood Flow Metab, 21*(10), 1133-1145.

Ayachit, U. (2015). *The ParaView Guide: A Parallel Visualization Application*: Kitware, Inc.

Basha, T. A., Akcakaya, M., Goddu, B., Berg, S., & Nezafat, R. (2015). Accelerated three-dimensional cine phase contrast imaging using randomly undersampled echo planar imaging with compressed sensing reconstruction. *NMR Biomed, 28*(1), 30-39.

Baumbach, G. L., & Heistad, D. D. (1988). Cerebral circulation in chronic arterial hypertension. *Hypertension, 12*(2), 89-95.

Beason-Held, L. L., Moghekar, A., Zonderman, A. B., Kraut, M. A., & Resnick, S. M. (2007). Longitudinal Changes in Cerebral Blood Flow in the Older Hypertensive Brain. *Stroke, 38*(6), 1766-1773.

Beauchet, O., Celle, S., Roche, F., Bartha, R., Montero-Odasso, M., Allali, G., & Annweiler, C. (2013). Blood pressure levels and brain volume reduction. *Journal of Hypertension, 31*(8), 1502-1516.

Benga, G., & Borza, T. (1995). Diffusional water permeability of mammalian red blood cells. *Comp Biochem Physiol B Biochem Mol Biol, 112*(4), 653-659.

Biswal, B. B. (2012). Resting state fMRI: a personal history. *Neuroimage, 62*(2), 938-944.

Blockley, N. P., Griffeth, V. E. M., Simon, A. B., & Buxton, R. B. (2015). Quantitative fMRI. In K. Uludag, K. Ugurbil, & L. Berliner (Eds.), *fMRI: From Nuclear Spins to Brain Functions* (pp. 215-243). Boston, MA: Springer US.

Bolar, D. S., Rosen, B. R., Sorensen, A. G., & Adalsteinsson, E. (2011). QUantitative Imaging of eXtraction of oxygen and TIssue consumption (QUIXOTIC) using venular-targeted velocity-selective spin labeling. *Magn Reson Med, 66*(6), 1550-1562.

Bulte, D. P., Kelly, M., Germuska, M., Xie, J., Chappell, M. A., Okell, T. W., Bright, M. G., & Jezzard, P. (2012). Quantitative measurement of cerebral physiology using respiratory-calibrated MRI. *Neuroimage, 60*(1), 582-591.

Bush, A. M., Borzage, M., Choi, S., Coates, T., & Wood, J. C. (2014). Elevated Cerebral Metabolic Oxygen Consumption in Sickle Cell Disease. *Blood, 124*(21), 2706-2706.

Chen, J. J., & Pike, G. B. (2009). Human whole blood T2 relaxometry at 3 Tesla. *Magn Reson Med, 61*(2), 249-254.

Chobanian, A. V., Bakris, G. L., Black, H. R., Cushman, W. C., Green, L. A., Izzo, J. L., Jr., Jones, D. W., Materson, B. J., Oparil, S., Wright, J. T., Jr., Roccella, E. J., National Heart, L., Blood Institute Joint National

Committee on Prevention, D. E., Treatment of High Blood, P., & National High Blood Pressure Education Program Coordinating, C. (2003). The Seventh Report of the Joint National Committee on Prevention, Detection, Evaluation, and Treatment of High Blood Pressure: the JNC 7 report. *JAMA, 289*(19), 2560-2572.

Cirillo, M., Laurenzi, M., Trevisan, M., & Stamler, J. (1992). Hematocrit, blood pressure, and hypertension. The Gubbio Population Study. *Hypertension, 20*(3), 319-326.

Davis, T. L., Kwong, K. K., Weisskoff, R. M., & Rosen, B. R. (1998). Calibrated functional MRI: mapping the dynamics of oxidative metabolism. *Proc Natl Acad Sci U S A, 95*(4), 1834-1839.

DeCarli, C., Miller, B. L., Swan, G. E., Reed, T., Wolf, P. A., Garner, J., Jack, L., & Carmelli, D. (1999). Predictors of brain morphology for the men of the NHLBI twin study. *Stroke, 30*(3), 529-536.

Derdeyn, C. P., Videen, T. O., Grubb, R. L., Jr., & Powers, W. J. (2001). Comparison of PET oxygen extraction fraction methods for the prediction of stroke risk. *J Nucl Med, 42*(8), 1195-1197.

Ding, Y., Mason, R. P., McColl, R. W., Yuan, Q., Hallac, R. R., Sims, R. D., & Weatherall, P. T. (2013). Simultaneous measurement of tissue oxygen level-dependent (TOLD) and blood oxygenation level-dependent (BOLD) effects in abdominal tissue oxygenation level studies. *J Magn Reson Imaging, 38*(5), 1230-1236.

Fan, A. P., Bilgic, B., Gagnon, L., Witzel, T., Bhat, H., Rosen, B. R., & Adalsteinsson, E. (2014). Quantitative oxygenation venography from MRI phase. *Magn Reson Med, 72*(1), 149-159.

Fernandez-Seara, M. A., Techawiboonwong, A., Detre, J. A., & Wehrli, F. W. (2006). MR susceptometry for measuring global brain oxygen extraction. *Magn Reson Med, 55*(5), 967-973.

Frank, L. R., Crawley, A. P., & Buxton, R. B. (1992). Elimination of oblique flow artifacts in magnetic resonance imaging. *Magn Reson Med, 25*(2), 299-307.

Fujishima, M., Ibayashi, S., Fujii, K., & Mori, S. (1995). Cerebral blood flow and brain function in hypertension. *Hypertens Res, 18*(2), 111-117.

Gasecki, D., Kwarciany, M., Nyka, W., & Narkiewicz, K. (2013). Hypertension, brain damage and cognitive decline. *Curr Hypertens Rep, 15*(6), 547-558.

Gauthier, C. J., & Hoge, R. D. (2012). Magnetic resonance imaging of resting OEF and CMRO(2) using a generalized calibration model for hypercapnia and hyperoxia. *Neuroimage, 60*(2), 1212-1225.

Ge, Y., Zhang, Z., Lu, H., Tang, L., Jaggi, H., Herbert, J., Babb, J. S., Rusinek, H., & Grossman, R. I. (2012). Characterizing brain oxygen metabolism in patients with multiple sclerosis with T2-relaxation-under-spin-tagging MRI. *J Cereb Blood Flow Metab, 32*(3), 403-412.

Gibbs, E. L., Lennox, W. G., Nims, L. F., & Gibbs, F. A. (1942). Arterial and cerebral venous blood - Arterial-venous differences in man. *Journal of Biological Chemistry, 144*(2), 325-332.

Gideon, P., Thomsen, C., Gjerris, F., Sorensen, P. S., Stahlberg, F., & Henriksen, O. (1996). Measurement of blood flow in the superior sagittal sinus in healthy volunteers, and in patients with normal pressure hydrocephalus and idiopathic intracranial hypertension with phase-contrast cine MR imaging. *Acta Radiol, 37*(2), 171-176.

Gopal, K. V., Thomas, B. P., Mao, D., & Lu, H. (2015). Efficacy of Carnitine in Treatment of Tinnitus: Evidence from Audiological and MRI Measures—A Case Study. *Journal of the American Academy of Audiology, 26*(3), 311-324.

Gopal, K. V., Thomas, B. P., Nandy, R., Mao, D., & Lu, H. (2017). Potential Audiological and MRI Markers of Tinnitus. *Journal of the American Academy of Audiology, In press*.

Gorelick, P. B., Scuteri, A., Black, S. E., Decarli, C., Greenberg, S. M., Iadecola, C., Launer, L. J., Laurent, S., Lopez, O. L., Nyenhuis, D., Petersen, R. C., Schneider, J. A., Tzourio, C., Arnett, D. K., Bennett, D. A., Chui, H. C., Higashida, R. T., Lindquist, R., Nilsson, P. M.,

Roman, G. C., Sellke, F. W., Seshadri, S., American Heart Association Stroke Council, C. o. E., Prevention, C. o. C. N. C. o. C. R., Intervention, Council on Cardiovascular, S., & Anesthesia. (2011). Vascular contributions to cognitive impairment and dementia: a statement for healthcare professionals from the american heart association/american stroke association. *Stroke, 42*(9), 2672-2713.

Grubb, R. L., Jr., Raichle, M. E., Eichling, J. O., & Ter-Pogossian, M. M. (1974). The effects of changes in PaCO2 on cerebral blood volume, blood flow, and vascular mean transit time. *Stroke, 5*(5), 630-639.

Guo, J., & Wong, E. C. (2012). Venous oxygenation mapping using velocity-selective excitation and arterial nulling. *Magn Reson Med, 68*(5), 1458-1471.

Gupta, A., Baradaran, H., Schweitzer, A. D., Kamel, H., Pandya, A., Delgado, D., Wright, D., Hurtado-Rua, S., Wang, Y., & Sanelli, P. C. (2014). Oxygen extraction fraction and stroke risk in patients with carotid stenosis or occlusion: a systematic review and meta-analysis. *AJNR Am J Neuroradiol, 35*(2), 250-255.

Haacke, E. M., Brown, R. W., Thompson, M. R., & Venkatesan, R. (1999). *Magnetic resonance imaging : physical principles and sequence design*. New York: Wiley.

Hafkenschiel, J. H., Crumpton, C. W., & Friedland, C. K. (1954). Cerebral oxygen consumption in essential hypertension; constancy with age, severity of the disease, sex, and variations of blood constituents, as observed in 101 patients. *J Clin Invest, 33*(1), 63-68.

Hallac, R. R., Zhou, H., Pidikiti, R., Song, K., Stojadinovic, S., Zhao, D., Solberg, T., Peschke, P., & Mason, R. P. (2014). Correlations of noninvasive BOLD and TOLD MRI with pO2 and relevance to tumor radiation response. *Magn Reson Med, 71*(5), 1863-1873.

He, X., & Yablonskiy, D. A. (2007). Quantitative BOLD: mapping of human cerebral deoxygenated blood volume and oxygen extraction fraction: default state. *Magn Reson Med, 57*(1), 115-126.

Heron, M. (2016). Deaths: Leading Causes for 2014. *Natl Vital Stat Rep, 65*(5), 1-96.

Hoge, R. D., Atkinson, J., Gill, B., Crelier, G. R., Marrett, S., & Pike, G. B. (1999). Linear coupling between cerebral blood flow and oxygen consumption in activated human cortex. *Proc Natl Acad Sci U S A, 96*(16), 9403-9408.

Iadecola, C., & Davisson, R. L. (2008). Hypertension and cerebrovascular dysfunction. *Cell Metab, 7*(6), 476-484.

Ibaraki, M., Miura, S., Shimosegawa, E., Sugawara, S., Mizuta, T., Ishikawa, A., & Amano, M. (2008). Quantification of cerebral blood flow and oxygen metabolism with 3-dimensional PET and 15O: validation by comparison with 2-dimensional PET. *J Nucl Med, 49*(1), 50-59.

Ishii, K., Kitagaki, H., Kono, M., & Mori, E. (1996). Decreased medial temporal oxygen metabolism in Alzheimer's disease shown by PET. *J Nucl Med, 37*(7), 1159-1165.

Jain, V., Buckley, E. M., Licht, D. J., Lynch, J. M., Schwab, P. J., Naim, M. Y., Lavin, N. A., Nicolson, S. C., Montenegro, L. M., Yodh, A. G., & Wehrli, F. W. (2014). Cerebral oxygen metabolism in neonates with congenital heart disease quantified by MRI and optics. *J Cereb Blood Flow Metab, 34*(3), 380-388.

Jordan, L. C., Gindville, M. C., Scott, A. O., Juttukonda, M. R., Strother, M. K., Kassim, A. A., Chen, S. C., Lu, H., Pruthi, S., Shyr, Y., & Donahue, M. J. (2016). Non-invasive imaging of oxygen extraction fraction in adults with sickle cell anaemia. *Brain, 139*(Pt 3), 738-750.

Krishnamurthy, L. C., Liu, P., Ge, Y., & Lu, H. (2014a). Vessel-specific quantification of blood oxygenation with T2-relaxation-under-phase-contrast MRI. *Magn Reson Med, 71*(3), 978-989.

Krishnamurthy, L. C., Liu, P., Xu, F., Uh, J., Dimitrov, I., & Lu, H. (2014b). Dependence of blood T(2) on oxygenation at 7 T: in vitro calibration and in vivo application. *Magn Reson Med, 71*(6), 2035-2042.

Krishnamurthy, L. C., Mao, D., King, K. S., & Lu, H. (2016). Correction and optimization of a T2-based approach to map blood oxygenation in small cerebral veins. *Magn Reson Med, 75*(3), 1100-1109.

Leenders, K. L. (1994). PET: blood flow and oxygen consumption in brain tumors. *J Neurooncol, 22*(3), 269-273.

Liu, P., Dimitrov, I., Andrews, T., Crane, D. E., Dariotis, J. K., Desmond, J., Dumas, J., Gilbert, G., Kumar, A., Maclntosh, B. J., Tucholka, A., Yang, S., Xiao, G., & Lu, H. (2016). Multisite evaluations of a T2 - relaxation-under-spin-tagging (TRUST) MRI technique to measure brain oxygenation. *Magn Reson Med, 75*(2), 680-687.

Liu, P., Lu, H., Filbey, F. M., Tamminga, C. A., Cao, Y., & Adinoff, B. (2014). MRI assessment of cerebral oxygen metabolism in cocaine-addicted individuals: hypoactivity and dose dependence. *NMR Biomed, 27*(6), 726-732.

Lu, H., & Ge, Y. (2008). Quantitative evaluation of oxygenation in venous vessels using T2-Relaxation-Under-Spin-Tagging MRI. *Magn Reson Med*, *60*(2), 357-363.

Lu, H., Liu, P., Yezhuvath, U., Cheng, Y., Marshall, O., & Ge, Y. (2014). MRI mapping of cerebrovascular reactivity via gas inhalation challenges. *J Vis Exp*(94).

Lu, H., Xu, F., Grgac, K., Liu, P., Qin, Q., & van Zijl, P. (2012). Calibration and validation of TRUST MRI for the estimation of cerebral blood oxygenation. *Magn Reson Med, 67*(1), 42-49.

Lu, H., Xu, F., Rodrigue, K. M., Kennedy, K. M., Cheng, Y., Flicker, B., Hebrank, A. C., Uh, J., & Park, D. C. (2011). Alterations in cerebral metabolic rate and blood supply across the adult lifespan. *Cereb Cortex, 21*(6), 1426-1434.

Lu, W., Yu, H., Shimakawa, A., Alley, M., Reeder, S. B., & Hargreaves, B. A. (2008). Water-fat separation with bipolar multiecho sequences. *Magn Reson Med*, *60*(1), 198-209.

Macmillan, C. S., & Andrews, P. J. (2000). Cerebrovenous oxygen saturation monitoring: practical considerations and clinical relevance. *Intensive Care Med, 26*(8), 1028-1036.

Matsumoto, K.-i., Bernardo, M., Subramanian, S., Choyke, P., Mitchell, J. B., Krishna, M. C., & Lizak, M. J. (2006). MR assessment of changes of tumor in response to hyperbaric oxygen treatment. *Magnetic Resonance in Medicine, 56*(2), 240-246.

Mintun, M. A., Raichle, M. E., Martin, W. R., & Herscovitch, P. (1984). Brain oxygen utilization measured with O-15 radiotracers and positron emission tomography. *J Nucl Med, 25*(2), 177-187.

Mori, S., Wu, D., Ceritoglu, C., Li, Y., Kolasny, A., Vaillant, M. A., Faria, A. V., Oishi, K., & Miller, M. I. (2016). MRICloud: Delivering High-Throughput MRI Neuroinformatics as Cloud-Based Software as a Service. *Computing in Science & Engineering, 18*(5), 21-35.

Muller, M., van der Graaf, Y., Visseren, F. L., Mali, W. P. T. M., & Geerlings, M. I. (2012). Hypertension and longitudinal changes in cerebral blood flow: The SMART-MR study. *Annals of Neurology, 71*(6), 825-833.

Murkin, J. M., & Arango, M. (2009). Near-infrared spectroscopy as an index of brain and tissue oxygenation. *British Journal of Anaesthesia, 103*(Supplement 1), i3-i13.

Nagata, K., Kondoh, Y., Atchison, R., Sato, M., Satoh, Y., Watahiki, Y., Hirata, Y., & Yokoyama, E. (2000). Vascular and metabolic reserve in Alzheimer's disease. *Neurobiol Aging, 21*(2), 301-307.

Neelavalli, J., Jella, P. K., Krishnamurthy, U., Buch, S., Haacke, E. M., Yeo, L., Mody, S., Katkuri, Y., Bahado-Singh, R., Hassan, S. S., Romero, R., & Thomason, M. E. (2014). Measuring venous blood oxygenation in fetal brain using susceptibility-weighted imaging. *J Magn Reson Imaging, 39*(4), 998-1006.

Nwankwo, T., Yoon, S. S., Burt, V., & Gu, Q. (2013). Hypertension among adults in the United States: National Health and Nutrition Examination Survey, 2011-2012. *NCHS Data Brief*(133), 1-8.

Oldendorf, W. H., Kitano, M., Shimizu, S., & Oldendorf, S. Z. (1965). Hematocrit of the human cranial blood pool. *Circ Res, 17*(6), 532-539.

Pascual, J. M., Campistol, J., & Gil-Nagel, A. (2008). Epilepsy in inherited metabolic disorders. *Neurologist, 14*(6 Suppl 1), S2-S14.

Pascual, J. M., Liu, P., Mao, D., Kelly, D. I., Hernandez, A., Sheng, M., Good, L. B., Ma, Q., Marin-Valencia, I., Zhang, X., Park, J. Y., Hynan, L. S., Stavinoha, P., Roe, C. R., & Lu, H. (2014a). Triheptanoin for Glucose Transporter Type I Deficiency (G1D). *JAMA Neurology, 71*(10), 1255.

Pascual, J. M., Liu, P., Mao, D., Kelly, D. I., Hernandez, A., Sheng, M., Good, L. B., Ma, Q., Marin-Valencia, I., Zhang, X., Park, J. Y., Hynan, L. S., Stavinoha, P., Roe, C. R., & Lu, H. (2014b). Triheptanoin for glucose transporter type I deficiency (G1D): modulation of human ictogenesis, cerebral metabolic rate, and cognitive indices by a food supplement. *JAMA Neurol, 71*(10), 1255-1265.

Peng, S. L., Ravi, H., Sheng, M., Thomas, B. P., & Lu, H. (2017). Searching for a truly "iso-metabolic" gas challenge in physiological MRI. *J Cereb Blood Flow Metab, 37*(2), 715-725.

Qin, Q., Grgac, K., & van Zijl, P. C. (2011). Determination of whole-brain oxygen extraction fractions by fast measurement of blood T(2) in the jugular vein. *Magn Reson Med, 65*(2), 471-479.

Raichle, M. E., MacLeod, A. M., Snyder, A. Z., Powers, W. J., Gusnard, D. A., & Shulman, G. L. (2001). A default mode of brain function. *Proc Natl Acad Sci U S A, 98*(2), 676-682.

Raz, N. (2005). Regional Brain Changes in Aging Healthy Adults: General Trends, Individual Differences and Modifiers. *Cerebral Cortex, 15*(11), 1676-1689.

Raz, N., Rodrigue, K. M., & Acker, J. D. (2003). Hypertension and the brain: vulnerability of the prefrontal regions and executive functions. *Behav Neurosci, 117*(6), 1169-1180.

Raz, N., Rodrigue, K. M., & Haacke, E. M. (2007). Brain aging and its modifiers: insights from in vivo neuromorphometry and susceptibility weighted imaging. *Ann N Y Acad Sci, 1097*, 84-93.

Remmele, S., Sprinkart, A. M., Müller, A., Träber, F., von Lehe, M., Gieseke, J., Flacke, S., Willinek, W. A., Schild, H. H., Sénégas, J., Keupp, J., & Mürtz, P. (2013). Dynamic and simultaneous MR measurement ofR1andR2* changes during respiratory challenges for the assessment of blood and tissue oxygenation. *Magnetic Resonance in Medicine, 70*(1), 136-146.

Sarelius, I. H., & Duling, B. R. (1982). Direct measurement of microvessel hematocrit, red cell flux, velocity, and transit time. *Am J Physiol, 243*(6), H1018-1026.

Scheeren, T. W., Schober, P., & Schwarte, L. A. (2012). Monitoring tissue oxygenation by near infrared spectroscopy (NIRS): background and current applications. *J Clin Monit Comput, 26*(4), 279-287.

Schell, R. M., & Cole, D. J. (2000). Cerebral monitoring: jugular venous oximetry. *Anesth Analg, 90*(3), 559-566.

Sheng, M., Liu, P., Mao, D., & Lu, H. (2017). Hyperoxia suppresses resting-state electroencephalography (EEG) activity and causes temporal delays in task-evoked potentials. *PLoS ONE, Accepted*.

Sheng, M., Lu, H., Liu, P., Thomas, B. P., & McAdams, C. J. (2015). Cerebral perfusion differences in women currently with and recovered from anorexia nervosa. *Psychiatry Res, 232*(2), 175-183.

Silvennoinen, M. J., Clingman, C. S., Golay, X., Kauppinen, R. A., & van Zijl, P. C. (2003). Comparison of the dependence of blood R2 and R2* on oxygen saturation at 1.5 and 4.7 Tesla. *Magn Reson Med, 49*(1), 47-60.

Stolz, E., Kaps, M., Kern, A., Babacan, S. S., & Dorndorf, W. (1999). Transcranial color-coded duplex sonography of intracranial veins and sinuses in adults. Reference data from 130 volunteers. *Stroke, 30*(5), 1070-1075.

Strassburger, T. L., Lee, H. C., Daly, E. M., Szczepanik, J., Krasuski, J. S., Mentis, M. J., Salerno, J. A., DeCarli, C., Schapiro, M. B., & Alexander, G. E. (1997). Interactive effects of age and hypertension on volumes of brain structures. *Stroke, 28*(7), 1410-1417.

Swan, G. E., DeCarli, C., Miller, B. L., Reed, T., Wolf, P. A., Jack, L. M., & Carmelli, D. (1998). Association of midlife blood pressure to late-life cognitive decline and brain morphology. *Neurology, 51*(4), 986-993.

Tarazi, R. C., Frohlich, E. D., Dustan, H. P., Gifford, R. W., Jr., & Page, I. H. (1966). Hypertension and high hematocrit. Another clue to renal arterial disease. *Am J Cardiol, 18*(6), 855-858.

Thomas, B. P., Sheng, M., Tseng, B. Y., Tarumi, T., Martin-Cook, K., Womack, K. B., Cullum, M. C., Levine, B. D., Zhang, R., & Lu, H. (2016). Reduced global brain metabolism but maintained vascular function in amnestic mild cognitive impairment. *J Cereb Blood Flow Metab*.

Tung, K.-C., Uh, J., Mao, D., Xu, F., Xiao, G., & Lu, H. (2013). Alterations in resting functional connectivity due to recent motor task. *Neuroimage, 78*, 316-324.

Varela, M., Hajnal, J. V., Petersen, E. T., Golay, X., Merchant, N., & Larkman, D. J. (2011). A method for rapid in vivo measurement of blood T1. *NMR Biomed, 24*(1), 80-88.

Victor, R. G., Haley, R. W., Willett, D. L., Peshock, R. M., Vaeth, P. C., Leonard, D., Basit, M., Cooper, R. S., Iannacchione, V. G., Visscher, W. A., Staab, J. M., Hobbs, H. H., & Dallas Heart Study, I. (2004). The Dallas Heart Study: a population-based probability sample for the multidisciplinary study of ethnic differences in cardiovascular health. *Am J Cardiol, 93*(12), 1473-1480.

Wang, G.-Z., Belgard, T. G., Mao, D., Chen, L., Berto, S., Preuss, Todd M., Lu, H., Geschwind, Daniel H., & Konopka, G. (2015). Correspondence between Resting-State Activity and Brain Gene Expression. *Neuron, 88*(4), 659-666.

Wansapura, J. P., Holland, S. K., Dunn, R. S., & Ball, W. S., Jr. (1999). NMR relaxation times in the human brain at 3.0 tesla. *J Magn Reson Imaging*, *9*(4), 531-538.

Wise, R. G., Harris, A. D., Stone, A. J., & Murphy, K. (2013). Measurement of OEF and absolute CMRO2: MRI-based methods using interleaved and combined hypercapnia and hyperoxia. *Neuroimage, 83*, 135-147.

Wong, E., & Guo, J. (2013). VENTI: venous territory imaging using remote sensing. *Proc. Intl. Soc. Mag. Reson. Med., 21*, 103.

Wright, G. A., Hu, B. S., & Macovski, A. (1991). Estimating oxygen saturation of blood in vivo with MR imaging at 1.5 T. *J Magn Reson Imaging, 1*(3), 275-283.

Wu, W. C., Jain, V., Li, C., Giannetta, M., Hurt, H., Wehrli, F. W., & Wang, D. J. (2010). In vivo venous blood T1 measurement using inversion recovery true-FISP in children and adults. *Magn Reson Med, 64*(4), 1140-1147.

Xu, B., Liu, T., Spincemaille, P., Prince, M., & Wang, Y. (2014). Flow compensated quantitative susceptibility mapping for venous oxygenation imaging. *Magn Reson Med*, *72*(2), 438-445.

Xu, F., Ge, Y., & Lu, H. (2009). Noninvasive quantification of whole-brain cerebral metabolic rate of oxygen (CMRO2) by MRI. *Magn Reson Med*, *62*(1), 141-148.

Xu, F., Liu, P., Pascual, J. M., Xiao, G., & Lu, H. (2012). Effect of hypoxia and hyperoxia on cerebral blood flow, blood oxygenation, and oxidative metabolism. *J Cereb Blood Flow Metab, 32*(10), 1909-1918.

Xu, F., Uh, J., Brier, M. R., Hart, J., Jr., Yezhuvath, U. S., Gu, H., Yang, Y., & Lu, H. (2011). The influence of carbon dioxide on brain activity and metabolism in conscious humans. *J Cereb Blood Flow Metab*, *31*(1), 58-67.

Yablonskiy, D. A., & Haacke, E. M. (1994). Theory of NMR signal behavior in magnetically inhomogeneous tissues: the static dephasing regime. *Magn Reson Med, 32*(6), 749-763.

Yablonskiy, D. A., Sukstanskii, A. L., Luo, J., & Wang, X. (2013). Voxel spread function method for correction of magnetic field inhomogeneity effects in quantitative gradient-echo-based MRI. *Magn Reson Med*, *70*(5), 1283-1292.

Yamada, K., Naruse, S., Nakajima, K., Furuya, S., Morishita, H., Kizu, O., Maeda, T., Takeo, K., & Shimizu, K. (1997). Flow velocity of the cortical vein and its effect on functional brain MRI at 1.5T: preliminary results by cine-MR venography. *J Magn Reson Imaging*, *7*(2), 347-352.

Yao, H., Sadoshima, S., Ibayashi, S., Kuwabara, Y., Ichiya, Y., & Fujishima, M. (1992). Leukoaraiosis and dementia in hypertensive patients. *Stroke*, *23*(11), 1673-1677.

Zhao, J. M., Clingman, C. S., Narvainen, M. J., Kauppinen, R. A., & van Zijl, P. C. (2007). Oxygenation and hematocrit dependence of transverse relaxation rates of blood at 3T. *Magn Reson Med*, *58*(3), 592-597.

Zheng, G., Wen, J., Lu, H., Lou, Y., Pan, Z., Liu, W., Liu, H., Li, X., Zhang, Z., Chen, H., Kong, X., Luo, S., Jiang, X., Liu, Y., Zhang, Z., Zhang, L. J., & Lu, G. M. (2016). Elevated global cerebral blood flow, oxygen extraction fraction and unchanged metabolic rate of oxygen in young adults with end-stage renal disease: an MRI study. *Eur Radiol*, *26*(6), 1732-1741.